 Printed in China Communications in Theoretical Physics

Commun. Theor. Phys. **77** (2025) 055204 (25pp) https://doi.org/10.1088/1572-9494/ad9c3d
CSTR: 32041.14.CTP.ad9c3d

Editor's Suggestion

Gravitational waves from patterns of electroweak symmetry breaking: an effective perspective

Rong-Gen Cai[1,2,3,4,5,*], **Katsuya Hashino**[6,7,*], **Shao-Jiang Wang**[2,8,*] and **Jiang-Hao Yu**[2,3,4,5,*]

[1] Institute of Fundamental Physics and Quantum Technology, Ningbo University, Ningbo 315211, China
[2] CAS Key Laboratory of Theoretical Physics, Institute of Theoretical Physics, Chinese Academy of Sciences, Beijing 100190, China
[3] School of Physical Sciences, University of Chinese Academy of Sciences (UCAS), Beijing 100049, China
[4] School of Fundamental Physics and Mathematical Sciences, Hangzhou Institute for Advanced Study (HIAS), University of Chinese Academy of Sciences, Hangzhou 310024, China
[5] International Centre for Theoretical Physics Asia-Pacific, Beijing/Hangzhou, China
[6] Center for High Energy Physics, Peking University, Beijing 100871, China
[7] National Institute of Technology, Fukushima College, Nagao 30, Taira-Kamiarakawa, Iwaki, Fukushima 970-8034, Japan
[8] Asia Pacific Center for Theoretical Physics (APCTP), Pohang 37673, Korea

E-mail: cairg@itp.ac.cn, hashino@fukushima-nct.ac.jp, schwang@itp.ac.cn and jhyu@itp.ac.cn

Received 11 September 2024, revised 26 November 2024
Accepted for publication 27 November 2024
Published 6 March 2025

Abstract

The future space-borne gravitational wave (GW) detectors would provide a promising probe for the new physics beyond the standard model that admits the first-order phase transitions. The predictions for the GW background vary sensitively among different concrete particle physics models but also share a large degeneracy in the model buildings, which motivates an effective model description on the phase transition based on different patterns of the electroweak symmetry breaking (EWSB). In this paper, using the scalar N-plet model as a demonstration, we propose an effective classification for three different patterns of EWSB: (1) radiative symmetry breaking with classical scale invariance, (2) the Higgs mechanism in a generic scalar extension, and (3) higher-dimensional operators. We conclude that a strong first-order phase transition could be realized for (1) and (2) with a small quartic coupling and a small isospin of an additional N-plet field for the light scalar field model with and without the classical scale invariance, and (3) with a large mixing coupling between scalar fields and a large isospin of the N-plet field for the heavy scalar field model.

Keywords: first-order phase transition, gravitational wave, standard model, effective field theory

(Some figures may appear in colour only in the online journal)

1. Introduction

Despite the success of the standard model (SM) of particle physics [1] as a low-energy effective field theory (EFT), it is incomplete in describing the puzzles of dark energy, dark matter (DM), cosmic inflation and baryon asymmetry of our Universe (BAU). The proposed solutions might call for a larger symmetry group for ultraviolet (UV) completion, which should be broken into the SM symmetry group in our current epoch. Some of these symmetry breakings would trigger cosmic first-order phase

* Authors to whom any correspondence should be addressed.

transitions (FOPTs) (see [2] for a comprehensive review and [3] for a pedagogical lecture) proceeding by the bubble nucleations, bubble expansion and bubble collisions, which would generate a stochastic background of gravitational waves (GWs) (see [4, 5] for recent reviews from LISA Collaboration [6] and [7, 8] for earlier reviews from eLISA/NGO mission [9]; see also [10] for a brief review) transparent to our early Universe that is otherwise opaque to light for us to probe via electromagnetic waves if the FOPTs occur before the recombination epoch. Therefore, the GWs' detection serves as a promising and unique probe [11, 12] for the new physics [13, 14] beyond SM (BSM) with FOPTs.

Since the SM admits no FOPT but a cross-over transition due to a relatively heavy Higgs mass [15], any model buildings with FOPTs should go beyond SM. However, a clean separation for BSM new physics with FOPTs from those without FOPTs turns out to be difficult, so does a clear classification for various FOPT models. Usually the FOPT models could be naively classified into models extended with higher-dimensional operators [16–39], scalar singlet [40–73] /doublet [74–91]/triplet [92–104]/quadruplet [30], composite Higgs [18, 19, 105–117], supersymmetry (SUSY) [118–144], warp extra-dimensions [116, 117, 145–184], and dark/hidden sectors [113, 164, 171, 185–242], which, however, are actually overlapping with each other when focusing on the sector that actually induces an FOPT. Nevertheless, most of the FOPT models could be regarded effectively as some kind of scalar extensions of the SM, while other FOPT models with fermion extensions [243–247] are special on their own for triggering a PT, we therefore only focus on the scalar extensions of the SM.

On the other hand, some of the scalar extensions of the SM could be described and parametrized in the effective field theory (EFT) framework, in which the new particles are integrated out and only the SM degrees of freedom are kept. The EFT description was adopted before, particularly for the higher-dimensional-operator extensions of the SM, which characterize the effect on the low-energy degrees of freedom when we integrate out the heavy degrees of freedom. However, the EFT description is only valid in the presence of a clear separation of scales, which is in conflict with the relatively low scale of the new degrees of freedom so as to introduce a large correction to the SM Higgs potential [248] in order to trigger a PT. Exceptions could be made for the Higgs-singlet extension with tree-level matching, though the EFT description is at its most qualitative for the dimension-six extension. Recently, a new perspective on this SM EFT description is made if the potential barrier separating the two minimums is generated radiatively instead of the tree-level barrier [249]. Nevertheless, we have found in this paper that the difficulty of an EFT description for the FOPT models could be circumvented by introducing a large number of scalar fields in the *N*-plet scalar field model. Therefore, for the electroweak phase transition process, the EFT description for some scalar extensions is not enough since in many cases the new light degree of freedom would contribute to the thermal plasma and thus one cannot integrate it out during phase transition. See also [250–252] for the dimensionally reduced effective field theory and its applications on reducing the uncertainties from the renormalization scale dependence [253, 254] and the thermal bubble nucleation calculation [255–257].

In this paper we instead take an intermediate strategy that lays between the specific new physics model and EFT treatment. We utilize a simplified model to illustrate the features of the electroweak phase transition (EWPT), which we call the effective model description on the phase transition. In this description, to capture different patterns of the EWPT and to compare the difference between the new physics model and the EFT description, we propose a specific effective model description: the general model extends the SM with an isospin *N*-plet scalar field, of which the light scalar case consists of a model with classical scale invariance (CSI) (model I) and a model without CSI (model II), while the heavy scalar case is simply a model with higher-dimensional operators, for example, a dimension-six operator (model III). The above cases could describe the patterns of the electroweak symmetry breaking (EWSB) via, for example, (1) radiative symmetry breaking, (2) Higgs mechanism, and (3) EFT description of EWSB. Our effective model description already covers those scalar models with *N*-plet on the market, such as (1) singlet models including a real scalar singlet extension of SM (xSM), composite Higgs model like SO(6)/SO(5) model, extra dimension model like radion model, dilaton model; (2) doublet models including SUSY model like minimal supersymmetry model (MSSM), two Higgs doublet model (2HDM), minimal dark matter model; (3) triplet models including left-right model, Type-II seesaw model. In other perspective, our effective model description consists of the simplified models (effective models I and II) for the realistic models (SUSY, composite Higgs, etc.) and an EFT model (model III). Therefore, our effective model provides an effective description for the EWSB that could admit a FOPT with associated GWs.

Although the effective scalar models describe different EWSB patterns, they share the same form of the Higgs potential. Thus, utilizing the polynomial potential form, we could analyze how the FOPT is realized in different cases. To show the source of a sizable barrier for realizing the first-order EWPT, we consider the following polynomial potential form in each of the three models,

$$V_p = C_2\phi^2 + C_3\phi^3 + C_4\phi^4 + C_6\phi^6, \tag{1}$$

where ϕ is the order parameter in the effective potential, and C_n are the effective couplings of ϕ^n. The ϕ^2 and ϕ^4 term can appear in it at tree-level, on the other hand, the ϕ^6 term comes from the high dimensional operator in the model (III). The ϕ^3 is the source of the first-order phase transition in the models (I) and (II), and it can be produced by the thermal loop effects. Let us summarize the main features and also the main results of this work on realizing the FOPT in the forementioned three models:

- For model I, there are no massive parameters, and we consider the EWPT along a flat direction in the tree-level potential to avoid invalidating the perturbative analysis, and thus the potential form with finite temperature effects are roughly given by $V_p = C_2\phi^2 + C_3\phi^3 + C_4\phi^4$, where all terms are one-loop level effects coming from thermal loop effects and radiative corrections.

Table 1. The potential forms in the three types of the models where the EWSB occurs via (I) radiative symmetry breaking; (II) Higgs mechanism; (III) EFT description. Here, ϕ is order parameter, and C_n is the effective coupling of ϕ^n. The cubic term can be produced by thermal loop effects of bosons. To generate a sizable barrier, the cubic term will be negative in models I and II. In the model III, the quartic term can be negative to generate the barrier.

Model	$C_2\phi^2$	$C_3\phi^3$	$C_4\phi^4$	$C_6\phi^6$
I	Loop	Loop	Loop	None
II	Tree	Loop	Tree	None
III	Tree	Loop	Tree	Tree

- For model II, there are massive parameters in the Lagrangian unlike the model I. The potential of this model is still roughly given by $V_p = C_2\phi^2 + C_3\phi^3 + C_4\phi^4$ but the tree-level effects are now in ϕ^2 and ϕ^4 terms.
- For model III, the high dimensional operator shows up in the potential $V_p = C_2\phi^2 + C_3\phi^3 + C_4\phi^4 + C_6\phi^6$, where the tree-level effects are in ϕ^2, ϕ^4 and ϕ^6 terms.

The main contributions to $C_n\phi^n$ in each of these models are summarized in Table 1. In the case of model I, not only the C_3 term but also the C_2 and C_4 terms are from loop level effects, and then the strongly first-order EWPT can be easily realized. On the other hand, the model II receives tree-level effects from the C_2 and C_4 terms. The source of the barrier for models I and II is the negative C_3 term from the thermal loop effects of bosons. Model III has the high dimensional operator C_6, and thus we can have a negative C_4 term to generate a sizable barrier. That is a different point from models I and II.

The outline of this paper is as follows: in section 2, we introduce our effective model description, whose effective potentials are detailed in section 3. The resulted GWs from the FOPT models described above are extracted in a way depicted in section 4. The FOPT predictions are summarized in section 5. Lastly, section 6 is devoted for conclusions and discussions. Appendix A provides some details on the model without CSI.

2. Effective models

We focus on the model with an additional isospin N-plet scalar field $\Phi_2 \sim (I_{\Phi_2}, Y_{\Phi_2})$ charged under $SU(2)_I \times U(1)_Y$ gauge symmetry, where I_{Φ_2} is the isospin and Y_{Φ_2} is the hypercharge. The scalar boson fields in the model are given by

$$\Phi_1 = \begin{pmatrix} G^{\pm}, \\ \frac{h + iG^0}{\sqrt{2}} \end{pmatrix}, \quad \Phi_2 = \frac{1}{\sqrt{2}} \begin{pmatrix} \phi_1 + \mathrm{i}\phi_{1,i} \\ \phi_2 + \mathrm{i}\phi_{2,i} \\ \vdots \\ \phi_N + \mathrm{i}\phi_{N,i} \end{pmatrix}, \tag{2}$$

where Φ_1 is the SM-like double scalar field and ϕ_n ($\phi_{n,i}$) is the real (imaginary) part of the additional isospin N-plet scalar field with $N \equiv 2I_{\Phi_2} + 1$. These scalar bosons Φ_1, Φ_2 have classical fields: $\langle\Phi_1\rangle/\sqrt{2}$ and $\langle\Phi_2\rangle/\sqrt{2}$, which are related to the real part of the neutral scalar field. We will discuss the testability from the GW detection for three types of the extended models instead on different patterns of the EWSB. These models are illustrated in figure 1. Two types of them are the model with a light scalar field: (I) the model with classical scale invariance (CSI), (II) the model without CSI. The last type of the model is (III) the model with the N-plet scalar field with TeV scale. These models can realize the EWSB via (I) radiative symmetry breaking, (II) Higgs mechanism and (III) EFT description of EWSB, respectively. For the simplicity of excluding the mixing terms, we assume Z_2 symmetry in such a way that the new scalar field is Z_2 odd while the others are Z_2 even.

2.1. The model with classical scale invariance

In the first type of the model, we impose CSI on the tree-level potential without any dimensional parameters, then the spontaneous EWSB is generated by radiative corrections [258] given later in (23). The Lagrangian of this model is

$$\mathcal{L} = \mathcal{L}_{\rm SM} + |D_\mu\Phi_2|^2 - V_0(\Phi_1, \Phi_2), \tag{3}$$

where $D_\mu = \partial_\mu - \mathrm{i}gT^aW_\mu^a - ig'Y_{\Phi_2}B_\mu/2$, g' and g are $\mathrm{U}(1)_Y$ and $\mathrm{SU}(2)_I$ gauge couplings, respectively, and T^a is the matrix for the generator of $\mathrm{SU}(2)_I$. The tree-level potential $V_0(\Phi_1, \Phi_2)$ is given by

$$V_0(\Phi_1, \Phi_2) = \lambda_1|\Phi_1|^4 + \lambda_2|\Phi_2|^4 + \lambda_{12}|\Phi_1|^2|\Phi_2|^2. \tag{4}$$

If the isospin I_{Φ_2} is $1/2$, then there are some mixing terms in the potential, such as $|\Phi_1^\dagger\Phi_2|^2$. For simplicity, we neglect such terms in the potential. According to [259, 260], there may be a flat direction in the tree-level potential to assure the valid perturbative analysis. If not, the large logarithmic term may show up in the one-loop correction via the renormalization scale, for example, this scale in the ϕ^4 theory is $Q \sim 3\lambda v e^{16\pi^2}$ [258]. Therefore, we assume a flat direction in the tree-level potential to avoid invalidating the perturbative analysis. The details of the effective potential will be discussed in section 3.

We mention here the constraints on this model. For simplicity, we assume that the additional scalar field Φ_2 does not couple to the SM fermions and does not have the vacuum-expectation-value (VEV). On the other hand, the isospin N-plet scalar field Φ_2 can interact with the SM gauge bosons. Then, the model is constrainted by the perturbative unitarity bound. According to [261], the isospin should be less than $7/2$. We assume that the additional scalar field does not couple to the SM-like fermion in our strategy. Therefore, the typical collider constraints on our model is not much tight. For the neutral heavy Higgs, since it does not mix with the SM Higgs and does not couple to the SM fermions, the only experimental constraint comes from the vector boson scattering process, and thus it is very loose. For the charged Higgs, due to their degenerate masses to the neutral one, experimental constraints can be relaxed except for the $h\gamma\gamma$ measurement. The additional charged scalar fields contribute to the Higgs coupling $h\gamma\gamma$ [262], which is given by 1.05 ± 0.09 [263]. We may distinguish models I and II by

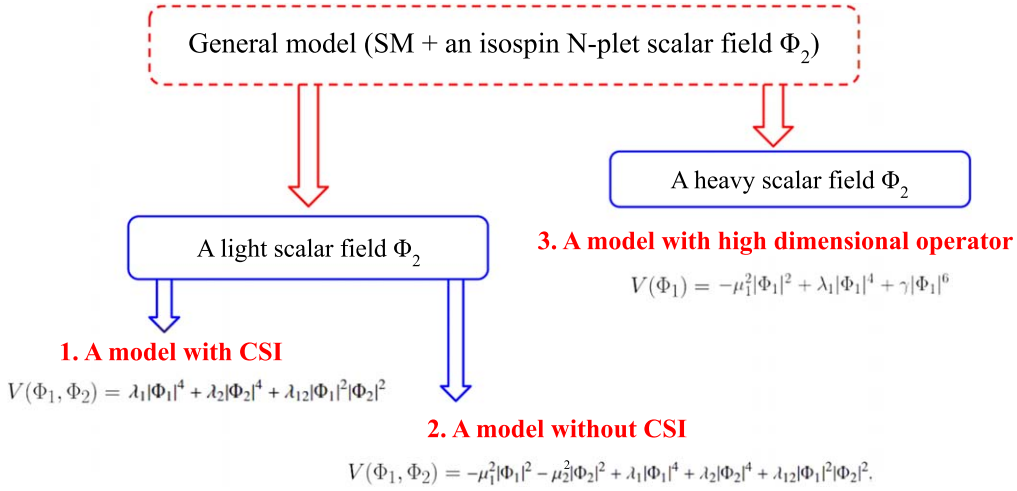

Figure 1. Our effective model description for some BSM models with FOPTs from a general model with an additional scalar field, which is either light or heavy consisting of (I) the light scalar model with CSI, (II) the light scalar model without CSI, (III) the heavy scalar model with high dimensional operator.

the results of the measurements and observation of the GW spectrum. In our work, we do not take into account the experimental constraints in the numerical analysis of the PT.

2.2. The model without classical scale invariance

In the model without CSI, there are mass parameters in the tree-level potential. The tree-level potential in this model is given as

$$V_0(\Phi_1,\Phi_2) = -\mu_1^2|\Phi_1|^2 - \mu_2^2|\Phi_2|^2 + \lambda_{12}|\Phi_1|^2|\Phi_2|^2 + \lambda_1|\Phi_1|^4 + \lambda_2|\Phi_2|^4, \quad (5)$$

where $\mu_1^2 > 0$ and $\lambda_1, \lambda_2 > 0$ for the stability of the tree-level potential. The effective potential of this model will be given later in (39).

Before discussing the effective potential with loop-corrections, we show the possible PT paths from the tree-level potential. At first, the extremal values in the potential are obtained by

$$\frac{\partial V_0(\langle\Phi_1\rangle,\langle\Phi_2\rangle)}{\partial\langle\Phi_1\rangle} = \frac{\partial V_0(\langle\Phi_1\rangle,\langle\Phi_2\rangle)}{\partial\langle\Phi_2\rangle} = 0, \quad (6)$$

which are solved by the following nine points in the field space as shown in figure 2,

$$(\langle\Phi_1\rangle,\langle\Phi_2\rangle) = (0,0),\quad \left(0,\pm\sqrt{\frac{\mu_2^2}{\lambda_2}}\right),\quad \left(\pm\sqrt{\frac{\mu_1^2}{\lambda_1}},0\right),$$
$$\left(\pm\sqrt{2\frac{\lambda_{12}\mu_2^2-2\lambda_2\mu_1^2}{\lambda_{12}^2-4\lambda_1\lambda_2}},\pm\sqrt{2\frac{\lambda_{12}\mu_2^2-2\lambda_2\mu_1^2}{\lambda_{12}^2-4\lambda_1\lambda_2}}\right),$$
$$\left(\pm\sqrt{2\frac{\lambda_{12}\mu_2^2-2\lambda_2\mu_1^2}{\lambda_{12}^2-4\lambda_1\lambda_2}},\mp\sqrt{2\frac{\lambda_{12}\mu_2^2-2\lambda_2\mu_1^2}{\lambda_{12}^2-4\lambda_1\lambda_2}}\right). \quad (7)$$

The green point is the origin in the potential, the blue points are $\langle\Phi_2\rangle \neq 0$ at zero temperature and the red and magenta points are along the $\langle\Phi_1\rangle$ and $\langle\Phi_2\rangle$ axes, respectively. When the red or blue point is minimum, the scalar field Φ_1 can have a VEV. In this work, we especially focus on the one-step phase transition along $\langle\Phi_1\rangle$ axis, because this path is the same as the CSI case. To realize the phase transition, we assume that the red point is at global minimum and the blue point is not minimum. We can assure such a situation by using the conditions for the determinants of the Hesse matrix and the height of the potential. The determinants of the Hesse matrix at the red, magenta and blue points are given by

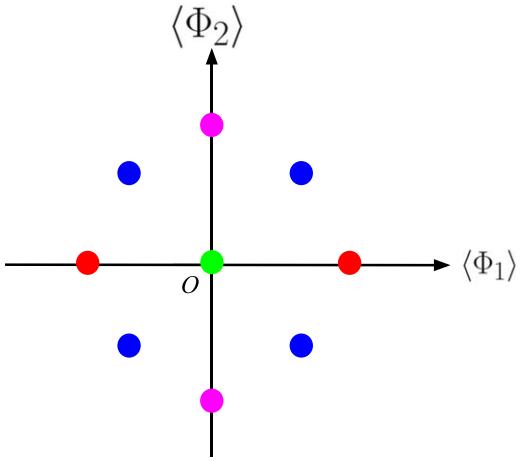

Figure 2. The extreme values of the tree-level potential of the model without CSI given by equation (7). In our analysis, the red (magenta) points will be global (local) minimum points and the blue points are saddle points.

$$\det[\mathcal{H}_{\rm red}] = \mu_1^2\left(\frac{\lambda_{12}\mu_1^2}{\lambda_1} - 2\mu_2^2\right), \quad (8)$$

$$\det[\mathcal{H}_{\rm mag}] = \mu_2^2\left(\frac{\lambda_{12}\mu_2^2}{\lambda_2} - 2\mu_1^2\right), \quad (9)$$

$$\det[\mathcal{H}_{\rm blue}] = -4\frac{(\lambda_{12}\mu_2^2 - 2\lambda_2\mu_1^2)(\lambda_{12}\mu_1^2 - 2\lambda_1\mu_2^2)}{\lambda_{12}^2 - 4\lambda_1\lambda_2}. \quad (10)$$

Also, the height of the potential at these points are given by

$$V_0(0,\sqrt{\mu_2^2/\lambda_2}) = -\mu_2^4/4\lambda_2, \quad (11)$$

$$V_0(\sqrt{\mu_1^2/\lambda_1}, 0) = -\mu_1^4/4\lambda_1$$
$$\times V_0\left(\sqrt{2\frac{\lambda_{12}\mu_2^2 - 2\lambda_2\mu_1^2}{\lambda_{12}^2 - 4\lambda_1\lambda_2}}, \sqrt{2\frac{\lambda_{12}\mu_2^2 - 2\lambda_2\mu_1^2}{\lambda_{12}^2 - 4\lambda_1\lambda_2}}\right)$$
$$= \frac{\lambda_1\mu_2^4 + \lambda_2\mu_1^4 - \lambda_{12}\mu_1^2\mu_2^2}{\lambda_{12}^2 - 4\lambda_1\lambda_2}. \quad (12)$$

The red point should be the lowest points among them. From that, we can obtain the following conditions

$$\frac{\lambda_{12}\mu_1^2}{\lambda_1} > 2\mu_2^2, \quad \frac{\lambda_{12}\mu_2^2}{\lambda_2} > 2\mu_1^2, \quad \mu_2^4/\lambda_2 < \mu_1^4/\lambda_1. \quad (13)$$

Since the potential with these conditions have two minima at magenta and red points, a two-step phase transition may be realized. In our numerical analysis, we distinguish the phase transition pattern and focus on the one-step phase transition to compare differences of the results between the models with and without CSI.

2.3. The model with dimension-six operator from Φ_2

In the last type of model, Φ_2 is assumed at the TeV scale and then we integrate out the additional scalar field. The tree-level potential in this model is given by

$$V_0(\Phi_1, \Phi_2) = -\mu_1^2|\Phi_1|^2 - \mu_2^2|\Phi_2|^2 + \lambda_1|\Phi_1|^4 + \lambda_2|\Phi_2|^4 + \lambda_{12}|\Phi_1|^2|\Phi_2|^2, \quad (14)$$

where μ_2 is at TeV scale. Otherwise, it is the same as the model without CSI. Then, we integrate out the heavy Φ_2 by loop-level matching [248, 264] in our analysis, and the effective Lagrangian for the SM-like Higgs boson h reads

$$\mathcal{L}_{\rm EFT}^{(6)} \sim \frac{1}{2}|\partial_\mu h|^2 - \left(-\frac{1}{2}a_2h^2 + \frac{1}{4}a_4h^4 + \frac{1}{6}a_6h^6\right) \quad (15)$$

with

$$a_2 = \mu_1^2, \quad (16)$$

$$a_4 = \lambda_1 - (1 + 2I_{\Phi_2})\frac{\lambda_{12}^2\mu_1^2}{9(4\pi)^2m_{\Phi_2}^2}, \quad (17)$$

$$a_6 = (1 + 2I_{\Phi_2})\frac{1}{(4\pi)^2m_{\Phi_2}^2}\left(\frac{\lambda_{12}^3}{8} + \frac{\lambda_{12}^2\lambda_1}{6}\right), \quad (18)$$

where $m_{\Phi_2}^2 = \mu_2^2 + \lambda_{12}v^2/2$ is the mass of the additional scalar field Φ_2. The effective potential with radiative corrections of this model is given later in (51).

We note that [248] suggests FOPT may be difficult in the model with a loop-level matching. According to their work, the FOPT requires the balancing between the dimension-four and dimension-six terms via $\frac{1}{4}\frac{U}{M^2}\frac{c_i\kappa^2}{16\pi^2} \sim \frac{m_h^2}{v^2} \sim 0.12$ with $c_i = 1/2$ (1) for a real (complex) scalar, where U and M correspond to the Higgs boson coupling to the heavy field and the mass parameter of the heavy field, respectively. On the other hand, the parameter region for a valid EFT expansion requires $2c_{\rm kin}v^2 < 1/2$ and $|a_8|v^2/a_6 < 1$, where $c_{\rm kin}$, a_6 and a_8 are high dimensional operators for kinetic term, dimension 6 and 8 terms, respectively. Since the conditions also limit to U/M^2 and $c_i\kappa^2/16\pi^2$. Therefore, they concluded that the FOPT cannot be generated in the model. At this time, we do not take into account other higher-dimensional operators involving the kinetic term.

3. Effective potentials

In this section, we discuss the forms of the effective potentials for our three effective model descriptions. To obtain the effective potential, we use the $\overline{\rm MS}$ scheme to absorb the divergence parts. Typically, the effective potential at the one-loop level reads

$$V_{\rm eff}(\langle\Phi_1\rangle, \langle\Phi_2\rangle, T) = V_0 + \sum_i \frac{n_i}{64\pi^2} M_i^4(\langle\Phi_1\rangle, \langle\Phi_2\rangle) \times \left(\ln\left(\frac{M_i^2(\langle\Phi_1\rangle, \langle\Phi_2\rangle)}{Q^2}\right) - c_i\right) + \Delta V_T, \quad (19)$$

where $M_i^2(\langle\Phi_1\rangle, \langle\Phi_2\rangle)$ is the field-dependent mass, n_i is the number of the degree of freedom, Q is the renormalization scale and c_i is $3/2$ ($i =$ boson, fermion) or $5/6$ ($i =$ gauge boson). The one-loop thermal contribution to the potential [265] is

$$\Delta V_T = \frac{T^4}{2\pi^2}\left\{\sum_{i=\rm bosons} n_i \int_0^\infty {\rm d}x\, x^2 \times \ln\left[1 - \exp\left(-\sqrt{x^2 + M_i^2(\langle\Phi_1\rangle, \langle\Phi_2\rangle, T)/T^2}\right)\right] + \sum_{i=\rm fermions} n_i \int_0^\infty {\rm d}x\, x^2 \times \ln\left[1 + \exp\left(-\sqrt{x^2 + M_i^2(\langle\Phi_1\rangle, \langle\Phi_2\rangle, T)/T^2}\right)\right]\right\}. \quad (20)$$

Here, we take into account the resummation effect $V_T^{\rm ring}$ obtained by [266]

$$V_T^{\rm ring} = \frac{T}{12\pi}\sum_{i=bosons} n_i((M_i^2(\langle\Phi_1\rangle, \langle\Phi_2\rangle, 0))^{3/2} - (M_i^2(\langle\Phi_1\rangle, \langle\Phi_2\rangle, T))^{3/2}), \quad (21)$$

where the thermal mass $M_i^2(\langle\Phi_1\rangle, \langle\Phi_2\rangle, T) = M_i^2(\langle\Phi_1\rangle, \langle\Phi_2\rangle) + \Pi_i$ receives the thermal correction from the thermal self-energy Π_i. Finally, the effective potential with finite temperature effects is obtained by

$$V_{\rm eff}(\langle\Phi_1\rangle, \langle\Phi_2\rangle, T) = V_0 + V_{1-\rm loop} + \Delta V_T + V_T^{\rm ring}. \quad (22)$$

The field-dependent masses in the effective potential of equation (19) and thermal correction Π_i in equation (22) depending on the details of model. Therefore we will discuss the form of the effective potential in each type of the model in the following.

3.1. The model with classical scale invariance

For the model (4) with CSI, the spontaneous EWSB occurs on the flat direction, which is assumed along $\langle\Phi_1\rangle$. Then, the effective potential is simply

$$V_{\rm eff}(\varphi, T = 0) = A\varphi^4 + B\varphi^4\ln\frac{\varphi^2}{Q^2}, \quad (23)$$

with A and B terms given by

$$A = \sum_i \frac{n_i}{64\pi^2 v^4} m_i^4 \left(\ln \frac{m_i^2}{v^2} - c_i \right), \quad B = \sum_i \frac{n_i}{64\pi^2 v^4} m_i^4, \tag{24}$$

where m_i is the mass of the field species i excluding the Higgs boson since this effect is at the one-loop level in this model case. n_i and c_i in the potential are given by $(n_W, n_Z, n_t, n_{\Phi_2}) = (6, 3, -12, 2(2I_{\Phi_2}+1))$ and $(c_W, c_Z, c_t) = (5/6, 5/6, 3/2, 3/2)$, respectively. Using the stationary condition, we have

$$\left. \frac{\partial V_{\rm eff}(\varphi, T=0)}{\partial \varphi} \right|_{\varphi=v} = \ln \frac{v^2}{Q^2} + \frac{1}{2} + \frac{A}{B} = 0, \tag{25}$$

where the renormalization scale Q is fixed. Because A and B are the loop effects, v can be large in contrast to the case of ϕ^4 theory. Also, the Higgs boson mass is obtained as

$$m_h^2 = \left. \frac{\partial^2 V_{\rm eff}(\varphi, T=0)}{\partial \varphi^2} \right|_{\varphi=v} = 8Bv^2, \tag{26}$$

from which we can obtain the additional scalar boson mass m_{Φ_2} as

$$m_{\Phi_2} = \frac{C}{(2(2I_{\Phi_2}+1))^{1/4}}, \tag{27}$$

$$C^4 \equiv 8\pi^2 v^2 m_h^2 - 3m_Z^4 - 6m_W^4 + 12m_t^4 \tag{28}$$

with $C = 543\,\text{GeV}$ determined by equation (10) of [267], and λ_{12} coupling is obtained via $m_{\Phi_2}^2 = \lambda_{12} v^2/2$ as

$$\lambda_{12} = \frac{\sqrt{2}\, C^2}{v^2 \sqrt{2I_{\Phi_2}+1}}. \tag{29}$$

With the help of equations (25) and (26), the one-loop effective potential at zero temperature could be obtained in terms of the renormalized mass of the Higgs boson as

$$V_{\rm eff}(\varphi, T=0) = \frac{m_h^2}{8v^2}\varphi^4 \left(\ln \frac{\varphi^2}{v^2} - \frac{1}{2} \right). \tag{30}$$

Since the loop effects are renormalized into the Higgs boson mass, the value of *hhh* coupling with one-loop effects does not depend on the model extension [267]. The field-dependent masses and resummation effects in the effective potential with finite temperature effects are

$$M_{\Phi_2}^2(\varphi, T) = \frac{m_{\Phi_2}^2}{v^2}\varphi^2 + T^2 \left((I_{\Phi_2}+1)\frac{\lambda_2}{6} + \frac{m_{\Phi_2}^2}{3v^2} + I_{\Phi_2}(I_{\Phi_2}+1)\frac{g^2}{4} + Y_{\Phi_2}^2 \frac{g'^2}{16} \right). \tag{31}$$

Similarly, the thermally corrected field-dependent masses of gauge bosons in the (W^1, W^2, W^3, B) basis are

$$M_g^{2(L,T)}(\varphi, T) = \frac{\varphi^2}{4} \begin{pmatrix} g^2 & & & \\ & g^2 & & \\ & & g^2 & gg' \\ & & gg' & g'^2 \end{pmatrix} + a_g^{(L,T)} T^2 \begin{pmatrix} \pi_W & & & \\ & \pi_W & & \\ & & \pi_W & \\ & & & \pi_B \end{pmatrix}, \tag{32}$$

where

$$M_W^2 = \frac{g^2}{4}\varphi^2, \quad M_{WB}^2 = \frac{gg'}{4}\varphi^2, \quad M_B^2 = \frac{g'^2}{4}\varphi^2, \tag{33}$$

$$\pi_W = \frac{g^2}{9} I_{\Phi_2}(1+I_{\Phi_2})(1+2I_{\Phi_2}) + \frac{11}{6}g^2, \tag{34}$$

$$\pi_B = \frac{g'^2 T^2}{12}(1+I_{\Phi_2}) Y_{\Phi_2}^2 + \frac{11}{6}g'^2, \ a_g^L = 1, \ a_T^T = 0. \tag{35}$$

The field-dependent mass of the fermion does not receive thermal correction in T^2 so that

$$M_t^2 = \frac{m_t^2}{v^2}\varphi^2. \tag{36}$$

In this model, there are three parameters in the tree-level potential,

$$\lambda_1, \ \lambda_2, \ \lambda_{12}, \tag{37}$$

where λ_1 is zero in order to assume a flat direction along $\langle \Phi_1 \rangle$ axis. According to equation (26), the isospin number I_{Φ_2} is related to the mass m_{Φ_2}. Therefore, the free parameters in the effective potential with finite temperature effects are in fact

$$I_{\Phi_2}, \ Y_{\Phi_2}, \ \lambda_2. \tag{38}$$

See Appendix B for the Landau pole in this model with CSI.

3.2. The model without classical scale invariance

For the model (5) without CSI, the effective potential is given by

$$V_{\rm eff}(\varphi_1, \varphi_2, T) = V_0 + \sum_i \frac{n_i}{64\pi^2} M_i^4 \left(\ln \frac{M_i^2}{Q^2} - c_i \right) + \Delta V_T, \tag{39}$$

where $\langle \Phi_1 \rangle = \varphi_1/\sqrt{2}$, $\langle \Phi_2 \rangle = \varphi_2/\sqrt{2}$ and

$$V_0 = -\frac{\mu_1^2}{2}\varphi_1^2 - \frac{\mu_2^2}{2}\varphi_2^2 + \frac{\lambda_1}{4}\varphi_1^4 + \frac{\lambda_2}{4}\varphi_2^4 + \frac{\lambda_{12}}{4}\varphi_1^2\varphi_2^2. \tag{40}$$

There are five model parameters in the tree-level potential and these parameters can be fixed in terms of the following parameters,

$$v, \ m_h, \ m_{\Phi_2}, \ \lambda_{12}, \ \lambda_2, \tag{41}$$

by the stationary conditions and the second derivatives of the effective potential. The details of them are given in Appendix A.

The field-dependent masses with resummation corrections from the finite temperature effects of the effective

potential are

$$M^2_{h,\Phi_2}(\varphi_1,\varphi_2,T)=\frac{1}{2}(M^2_{11}+M^2_{22} \mp\sqrt{(M^2_{11}-M^2_{22})^2+4M^2_{12}M^2_{21}}), \quad (42)$$

$$M^2_{N_1}(\varphi_1,\varphi_2,T)=-\mu_1^2+\lambda_1\varphi_1^2+\frac{\lambda_{12}}{2}\varphi_2^2 +T^2\Big((2I_{\Phi_2}+1)\frac{\lambda_{12}}{12} +\frac{\lambda_h}{4}+\frac{3g^2}{16}+\frac{g'^2}{16}+\frac{y_t^2}{4}\Big), \quad (43)$$

$$M^2_{N_2}(\varphi_1,\varphi_2,T)=-\mu_2^2+\lambda_2\varphi_2^2+\frac{\lambda_{12}}{2}\varphi_1^2 +T^2\Big(\frac{(I_{\Phi_2}+1)\lambda_2}{6}+\frac{\lambda_{12}}{6} +\frac{g^2}{4}(I^2_{\Phi_2}+I_{\Phi_2})+\frac{g'^2Y^2_{\Phi_2}}{16}\Big), \quad (44)$$

where

$$\begin{pmatrix}M^2_{11} & M^2_{12}\\ M^2_{21} & M^2_{22}\end{pmatrix}=\begin{pmatrix}-\mu_1^2+3\lambda_1\varphi_1^2+\frac{\lambda_{12}}{2}\varphi_2^2 & \lambda_{12}\varphi_1\varphi_2\\ \lambda_{12}\varphi_1\varphi_2 & -\mu_2^2+3\lambda_2\varphi_2^2+\frac{\lambda_{12}}{2}\varphi_1^2\end{pmatrix} +T^2\begin{pmatrix}(2I_{\Phi_2}+1)\frac{\lambda_{12}}{12}+\frac{\lambda_1}{4}+\frac{3g^2}{16}+\frac{g'^2}{16}+\frac{y_t^2}{4} & 0\\ 0 & \frac{(I_{\Phi_2}+1)\lambda_2}{6}+\frac{\lambda_{12}}{6}+\frac{g^2}{4}(I^2_{\Phi_2}+I_{\Phi_2})+\frac{g'^2Y^2_{\Phi_2}}{16}\end{pmatrix}. \quad (45)$$

Also the thermally corrected field-dependent masses of gauge bosons in the (W^1, W^2, W^3, B) basis are

$$M_g^{2(L,T)}=\begin{pmatrix}M_W^2 & & & \\ & M_W^2 & & \\ & & M_W^2 & M_{WB}^2\\ & & M_{WB}^2 & M_B^2\end{pmatrix} + a_g^{(L,T)}T^2\begin{pmatrix}\pi_W & & & \\ & \pi_W & & \\ & & \pi_W & \\ & & & \pi_B\end{pmatrix}, \quad (46)$$

where

$$M_W^2=\frac{g^2}{4}(\varphi_1^2+I_W^2\varphi_2^2),\quad M_{WB}^2=\frac{gg'}{4}(\varphi_1^2+Y^2_{\Phi_2}\varphi_2^2), \quad (47)$$

$$M_B^2=\frac{g'^2}{4}(\varphi_1^2+Y^2_{\Phi_2}\varphi_2^2),\quad a_g^L=1,\quad a_T^T=0, \quad (48)$$

$$\pi_W=\frac{g^2}{9}I_{\Phi_2}(1+I_{\Phi_2})(1+2I_{\Phi_2})+\frac{11}{6}g^2, \quad (49)$$

$$\pi_B=\frac{g'^2T^2}{12}(1+I_{\Phi_2})Y^2_{\Phi_2}+\frac{11}{6}g'^2. \quad (50)$$

In this model, the EWPT can be generated in multi-field space (φ_1, φ_2). We will focus on the path of the phase transition along φ_1 axis. Therefore, we will discuss the possibility of one-step and two-step PTs, and will especially focus on the path of the phase transition along φ_1 axis to discuss the distinction among the three types of models with one-step PT.

3.3. The model with dimension-six operator from Φ_2

For the effective model (15) after integrating out the heavy scalar sector from (14), the effective potential is

$$V_{\rm eff}(\varphi_1,T)=-\frac{1}{2}a_2\varphi_1^2+\frac{1}{4}a_4\varphi_1^4+\frac{1}{6}a_6\varphi_1^6 +\sum_i\frac{n_i}{64\pi^2}M_i^4\left(\ln\left(\frac{M_i^2}{Q^2}\right)-c_i\right)+\Delta V_T, \quad (51)$$

where a_2, a_4 and a_6 are given in equation (16), and the field-dependent mass of Higgs boson along with its thermal correction are

$$M_h^2(\varphi_1)=-a_2+3a_4\varphi_1^2+5a_6\varphi_1^4, \quad (52)$$

$$\Pi_h=T^2\left(\frac{a_4}{4}+\frac{3g^2}{16}+\frac{g'^2}{16}+\frac{y_t^2}{4}\right). \quad (53)$$

The thermally corrected field-dependent masses of gauge bosons in the (W^1, W^2, W^3, B) basis are

$$M_g^{2(L,T)}(\varphi,T)=\frac{\varphi^2}{4}\begin{pmatrix}g^2 & & & \\ & g^2 & & \\ & & g^2 & gg'\\ & & gg' & g'^2\end{pmatrix} + a_g^{(L,T)}T^2\begin{pmatrix}\pi_W & & & \\ & \pi_W & & \\ & & \pi_W & \\ & & & \pi_B\end{pmatrix}, \quad (54)$$

where

$$M_W^2=\frac{g^2}{4}\varphi_1^2,\quad M_{WB}^2=\frac{gg'}{4}\varphi_1^2,\quad M_B^2=\frac{g'^2}{4}\varphi_1^2, \quad (55)$$

$$\pi_W=\frac{11}{6}g^2,\quad \pi_B=\frac{11}{6}g'^2,\quad a_g^L=1,\quad a_T^T=0 \quad (56)$$

and the field-dependent mass of top quark is

$$M_t^2=\frac{m_t^2}{v^2}\varphi_1^2. \quad (57)$$

There are three new parameters in this potential, namely,

$$m^2_{\Phi_2},\ \lambda_{12},\ I_{\Phi_2}. \quad (58)$$

4. Gravitational waves

The GWs from the FOPTs serve as the promising probe for the new physics of BSM, including our EFT models of EWSB. In this section, we briefly outline the computation procedures to carry out our model constraints.

4.1. Phase-transition parameters

For an effective potential $V_{\rm eff}$ exhibiting a false vacuum ϕ_+ and a true vacuum ϕ_- separated by a potential barrier, a cosmological FOPT proceeds via stochastic nucleations of true vacuum bubbles followed by a rapid expansion until a successful percolation to fully complete the phase transition process. In this section, we describe the phase transition dynamics consisting of the bubble nucleation and bubble percolation, which could be determined by the thermodynamics of effective potential alone without reference to the microscopic physics that leads to the macroscopic hydrodynamics of bubble expansion.

4.1.1. Bounce action. The bubble nucleations of true vacuum bubbles at finite temperature admit stochastic emergences of the field configuration $\phi(r)$ connecting a true vacuum region $\phi(r=0)\equiv\phi_0\lesssim\phi_-$ (assuming $\phi_+<\phi_-$) to the asymptotic false vacuum region $\phi(r\to\infty)\equiv\phi_+$ in an $O(4)$-symmetric manner $\mathrm{d}s^2=\mathrm{d}r^2+r^2\mathrm{d}\Omega_3^2$ or an $O(3)$-symmetric manner $\mathrm{d}s^2=\mathrm{d}\tau^2+\mathrm{d}r^2+r^2\mathrm{d}\Omega_2^2$ depending on their maximum value of the nucleation rates [268–271]

$$\Gamma(T)=\max\left[T^4\left(\frac{S_3}{2\pi T}\right)^{\frac{3}{2}}\mathrm{e}^{-\frac{S_3}{T}},\frac{1}{R_0^4}\left(\frac{S_4}{2\pi}\right)\mathrm{e}^{-S_4}\right],\tag{59}$$

where the $O(4)$ bounce action

$$S_4=2\pi^2\int_0^\infty \mathrm{d}r\, r^3\times\left[\frac{1}{2}\left(\frac{\mathrm{d}\phi_B}{\mathrm{d}r}\right)^2+V_{\rm eff}(\phi_B,T)-V_{\rm eff}(\phi_+,T)\right]\tag{60}$$

is evaluated at the solution ϕ_B of the equation-of-motion

$$\frac{\mathrm{d}^2\phi}{\mathrm{d}r^2}+\frac{3}{r}\frac{\mathrm{d}\phi}{\mathrm{d}r}=\frac{\partial V_{\rm eff}}{\partial\phi},\quad \phi'(0)=0,\quad \phi(\infty)=\phi_+,\tag{61}$$

while the $O(3)$ bounce action

$$\frac{S_3}{T}=\frac{4\pi}{T}\int_0^\infty \mathrm{d}r\, r^2\times\left[\frac{1}{2}\left(\frac{\mathrm{d}\phi_B}{\mathrm{d}r}\right)^2+V_{\rm eff}(\phi_B,T)-V_{\rm eff}(\phi_+,T)\right]\tag{62}$$

is evaluated at the solution ϕ_B of the equation-of-motion

$$\frac{\mathrm{d}^2\phi}{\mathrm{d}r^2}+\frac{2}{r}\frac{\mathrm{d}\phi}{\mathrm{d}r}=\frac{\partial V_{\rm eff}}{\partial\phi},\quad \phi'(0)=0,\quad \phi(\infty)=\phi_+.\tag{63}$$

In the realistic estimations, the vacuum decay rate from S_4 usually dominates over the thermal decay rate from S_3/T at extremely low temperature when the potential barrier does not vanish even at $T=0$. R_0 is the bubble radius defined by $\phi_B(r=R_0)=(\phi_0-\phi_+)/2$.

4.1.2. Nucleation temperature. During the whole process of bubble nucleation, the false vacuum becomes unstable once the temperature drops below the critical temperature defined by

$$V_{\rm eff}(\phi_+,T_c)=V_{\rm eff}(\phi_-(T_c),T_c).\tag{64}$$

However, the bubble nucleation is only possible when the temperature further drops down to $T=T_i<T_c$ defined

$$\phi_B(r=0,T_i)=\phi_-(T_i)\tag{65}$$

due to the presence of the Hubble friction term in the bounce equation. Since then, one can count the number of nucleated bubbles in one Hubble volume during a given time elapse by

$$N(T(t))=\int_{t_i}^{t}\mathrm{d}t\frac{\Gamma(t)}{H^3}=\int_T^{T_i}\frac{\mathrm{d}T}{T}\frac{\Gamma(T)}{H(T)^4},\tag{66}$$

until the nucleation temperature $T_n<T_i$ defined by the moment when there is exactly one bubble nucleated in one Hubble volume,

$$N(T_n)=1.\tag{67}$$

4.1.3. Percolation temperature. The progress of the phase transition could be described by the expected volume fraction of the true-vacuum regions at time t [272–274],

$$I(t)=\frac{4\pi}{3}\int_{t_i}^{t}\mathrm{d}t'\,\Gamma(t')a(t')^3r(t,t')^3,\tag{68}$$

where $r(t,t')$ is the comoving radius of a bubble at t nucleated at an earlier time t',

$$r(t,t')\equiv\frac{R_0}{a(t')}+\int_{t'}^{t}\frac{v_w(\tilde{t})\mathrm{d}\tilde{t}}{a(\tilde{t})}\approx v_w\int_{t'}^{t}\frac{\mathrm{d}\tilde{t}}{a(\tilde{t})}.\tag{69}$$

Here, we omit the initial bubble radius R_0 and fix the time-dependent bubble wall velocity $v_w(t)$ at its terminal v_w. When the effects for the overlapping of true-vacuum bubbles and 'virtual bubbles' nucleated in the true-vacuum regions are taken into account, the fraction of regions that are still sitting at the false vacuum at time t could be approximated by the exponentiation of $I(t)$,

$$P(t)=\mathrm{e}^{-I(t)}.\tag{70}$$

A percolation temperature $T_p<T_n$ is therefore defined by a conventional estimation [24, 122, 274–276]

$$P(T_p)=1/e.\tag{71}$$

In what follows, the strength factor and characteristic length scale for determining the peak amplitude and frequency in the GW spectrum will be evaluated at the percolation temperature.

4.1.4. Strength factor. To characterize the total released latent heat into the plasma, a parameter α is defined by [274]

$$\alpha(T)=\frac{\Delta\rho_{\rm vac}(T)}{\rho_{\rm rad}(T)},\tag{72}$$

with the total released vacuum energy defined by

$$\begin{aligned}\Delta\rho_{\rm vac}(T) &= \rho(\phi_+, T) - \rho(\phi_-(T), T)\\ &= \Delta V_{\rm eff}(T) - T\frac{\partial \Delta V_{\rm eff}(T)}{\partial T}\end{aligned} \tag{73}$$

due to $\rho = \mathcal{F} + Ts = -p + T\frac{\partial p}{\partial T} = V_{\rm eff} - T\frac{\partial V_{\rm eff}}{\partial T}$ similar to the usual definition of latent heat $L(T_c) = \rho(\phi_+, T_c) - \rho(\phi_-(T_c), T_c)$ at critical temperature. Here, $\Delta V_{\rm eff}(T) \equiv V_{\rm eff}(\phi_+(T), T) - V_{\rm eff}(\phi_-(T), T)$ for short.

4.1.5. Characteristic length scale. The characteristic length scale R_* for the peak position of the GW spectrum is estimated from the inverse duration β of the phase transition via the average number density of bubbles as

$$R_* = n_B^{-1/3} = (8\pi)^{1/3} v_w \beta^{-1}, \tag{74}$$

where the inverse duration β of the phase transition is computed by expanding the nucleation rate around the percolation time,

$$\Gamma = {\rm e}^{\beta(t-t_p)+\cdots}, \quad P(t_p) = 1/e, \tag{75}$$

$$\beta = -\frac{\rm d}{{\rm d}t}\frac{S_3(t)}{T(t)}\bigg|_{t=t_p} = H(T)T\frac{\rm d}{{\rm d}T}\frac{S_3(T)}{T}\bigg|_{T=T_p}. \tag{76}$$

4.2. Gravitational wave spectrum

The GW spectrum from a FOPT consists of three contributions: the bubble wall collisions, the sound waves, and the magnetohydrodynamic (MHD) turbulences. The contribution from the MHD turbulences is usually sub-dominated and hence omitted in the current study. The contribution from the bubble wall collisions [277–281] only dominates the total GW spectrum when the bubble walls collide with each other while they are still rapidly accelerating. In most of the cases, the runaway wall expansion is highly unlikely, and they usually collide with each other long after having approached to the terminal velocity. Therefore, we only consider the contribution from the sound waves, which is well fitted numerically by [274, 282–286]

$$\begin{aligned}h^2\Omega_{\rm sw} = 8.5\times 10^{-6}&\left(\frac{100}{g_{\rm dof}}\right)^{\frac{1}{3}}\left(\frac{\kappa_v\alpha}{1+\alpha}\right)^2\left(\frac{H_*}{\beta}\right)v_w\\ &\times\frac{7^{\frac{7}{2}}(f/f_{\rm sw})^3}{(4+3(f/f_{\rm sw})^2)^{\frac{7}{2}}}\Upsilon(\tau_{\rm sw}),\end{aligned} \tag{77}$$

with the peak frequency

$$f_{\rm sw} = 1.9\times 10^{-5}\,{\rm Hz}\left(\frac{g_{\rm dof}}{100}\right)^{\frac{1}{6}}\frac{T_\star}{100{\rm GeV}}\frac{1}{v_w}\frac{\beta}{H_*}. \tag{78}$$

Here, the suppression factor Υ is only important for sufficiently long duration comparable to or even slightly larger than the Hubble time scale, which is also neglected in our current study. Furthermore, both the wall velocity v_w and efficiency factor of bulk fluid motions κ_v are also set to be unity for simplicity.

To quickly locate the parameter space with a promising detectability of the GW signals, we will first use the ratio ϕ_C/T_C at the critical temperature as a roughly estimation for the size of the strength factor [4, 287],

$$\alpha \sim \alpha_\infty \simeq 4.9\times 10^{-3}\left(\frac{\phi_*}{T_*}\right)^2, \tag{79}$$

which is a typically reliable estimation for most of the non-supercooling electroweak PTs since there are no new relativistic degrees of freedom or new particles with couplings to the Higgs comparable to those of the $SU(2)_L$ gauge bosons or top quark. To qualify the model detectability, the GWs signals $h^2\Omega_{\rm GW}(f)$ are compared to the sensitivity curves of some GW detectors $h^2\Omega_{\rm sen}(f)$ during the mission year $\mathcal{T}$ by the signal-to-noise ratio (SNR),

$${\rm SNR} = \sqrt{\mathcal{T}\int_{f_{\rm min}}^{f_{\rm max}}{\rm d}f\left[\frac{h^2\Omega_{\rm GW}(f)}{h^2\Omega_{\rm sen}(f)}\right]^2}. \tag{80}$$

5. Summary of results

In this section, we show the results for the effective model descriptions with three types of the EWSB: (I) the light scalar model with CSI, (II) the light scalar model without CSI, and (III) the heavy scalar model with a higher-dimensional operator after integrating out the additional heavy scalar. Besides the common SM parameters (v, m_h, m_W, m_Z, m_t, g, g', α_s, y_t), the new parameters in these three models are summarized below:

- For model I, there are five parameters (I_{Φ_2}, Y_{Φ_2}, λ_1, λ_2, λ_{12}) from the effective potential (23). By using the stationary condition, we can introduce the massive parameter EW vacuum by the dimensional transmutation [258]. From the second derivative of the potential, the λ_{12} is related to the SM effects, like equation (29). λ_1 is assumed to be zero for a flat direction along $\langle\Phi_1\rangle$ axis. Eventually, there are three free dimensionless parameters: (I_{Φ_2}, Y_{Φ_2}, λ_2).
- For model II, there are seven parameters (I_{Φ_2}, Y_{Φ_2}, μ_1, μ_2, λ_1, λ_2, λ_{12}) in the effective potential. With the stationary condition, the massive parameter μ_1 can be replaced by the EW VEV v. From the second derivatives of the potential, λ_1 and μ_2 parameters are given by the Higgs boson mass m_h and the additional scalar boson mass m_{Φ_2}. Eventually, there are five free parameters: (I_{Φ_2}, Y_{Φ_2}, λ_2, m_{Φ_2}, λ_{12}).
- For model III, there are five parameters (I_{Φ_2}, μ_1, m_{Φ_2}, λ_1, λ_{12}) from the tree-level potential (15), two of which, for example, μ_1 and λ_1, could be fixed by the EW vacuum normalization conditions in terms of the EW VEV v and the Higgs mass m_h, leaving behind three free parameters (I_{Φ_2}, m_{Φ_2}, λ_{12}).

Note that in models I and II, although the hypercharge Y_{Φ_2} is a free parameter, it does not significantly change the PT results since its effect is proportional to $(m_W - m_Z)$ via Daisy

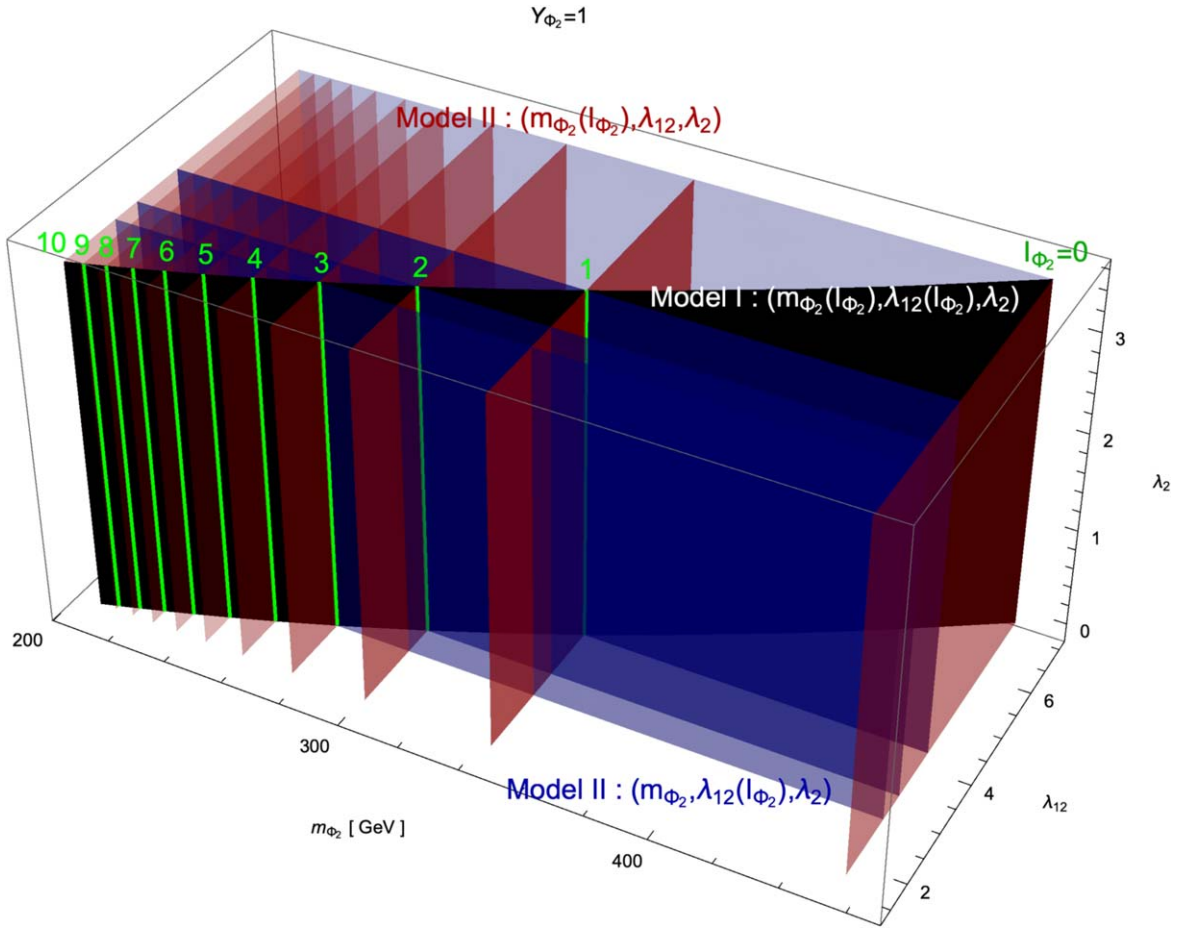

Figure 3. The presentation for a part of the effective models of interest in the parameter space supported by (m_{Φ_2}, λ_{12}, λ_2) with a fixed $Y_{\Phi_2} = 1$. The black strip is model I with both m_{Φ_2} and λ_{12} determined by I_{Φ_2} labeled in green. For model II, we take two illustrative examples with (1) the same m_{Φ_2} as model I but a free λ_{12} detached from I_{Φ_2} presented as red slices, and (2) the same λ_{12} as model I but a free m_{Φ_2} detached from I_{Φ_2} presented as blue slices.

diagram contributions. Thus, we take $Y_{\Phi_2} = 1$ as an illustrative example in the following PT analysis. For consistent comparison, we consider the models with common values for the shared free parameters. For example, the model I and model II can be compared in the parameter space of I_{Φ_2} and λ_2 for given choices of m_{Φ_2} and λ_{12} as illustrated in figure 3. The black plane in figure 3 corresponds to the parameter region for model I. The m_{Φ_2} is proportional to the λ_{12} in this model. Such a relation is given by a line in the plane of (m_{Φ_2}, λ_{12}. Since the λ_2, which corresponds to the z axis in this figure, is independent free parameter, the black plane in figure 3 corresponds to the parameter region for model I. The green lines are the I_{Φ_2} in model I. Since model II has five free parameters, the all free parameters in this model cannot be determined, even if the parameters have the same values as the CSI model. Such parameter regions correspond to the red and blue planes.

5.1. The model with classical scale invariance

In this section, we first show the value of ϕ_C/T_C for model I in the first panel of figure 4 to see which part of parameter space could produce detectable GWs. The horizontal axis is the quartic coupling λ_2 and the vertical axis is the isospin I_{Φ_2} of the additional scalar boson fields. It is easy to see that the value of ϕ_C/T_C is large for either small isospin I_{Φ_2} or small λ_2 coupling. This result of ϕ_C/T_C is different from our intuition since the strongly FOPT can be typically realized by adding a large number of additional scalar boson fields into the model, which corresponds to a large isospin I_{Φ_2}. In the model with CSI, the number of additional scalar boson fields is related to the Higgs boson mass via equation (26). Then, the ϕ_C/T_C without ring diagram contribution is roughly estimated by

$$\frac{\phi_C}{T_C} = \frac{E}{\lambda_2} \propto I_{\Phi_2}^{1/4}. \tag{81}$$

On the other hand, the ring diagram contribution has $I_{\Phi_2}^2$-dependence in equation (45), therefore, ϕ_C/T_C becomes small through large ring diagram contributions from large $I_{\Phi_2}^2$ value.

The PT parameters T_n, α and β/H are shown in the last three panels of figure 4, respectively. From these parameters, we can describe the GW spectrum from the FOPT. The SNR for the testability of this model with CSI is shown in figure 5 with respect to the future space-borne GW detectors LISA, the DECi-hertz Interferometer Gravitational Wave Observatory (DECIGO), and

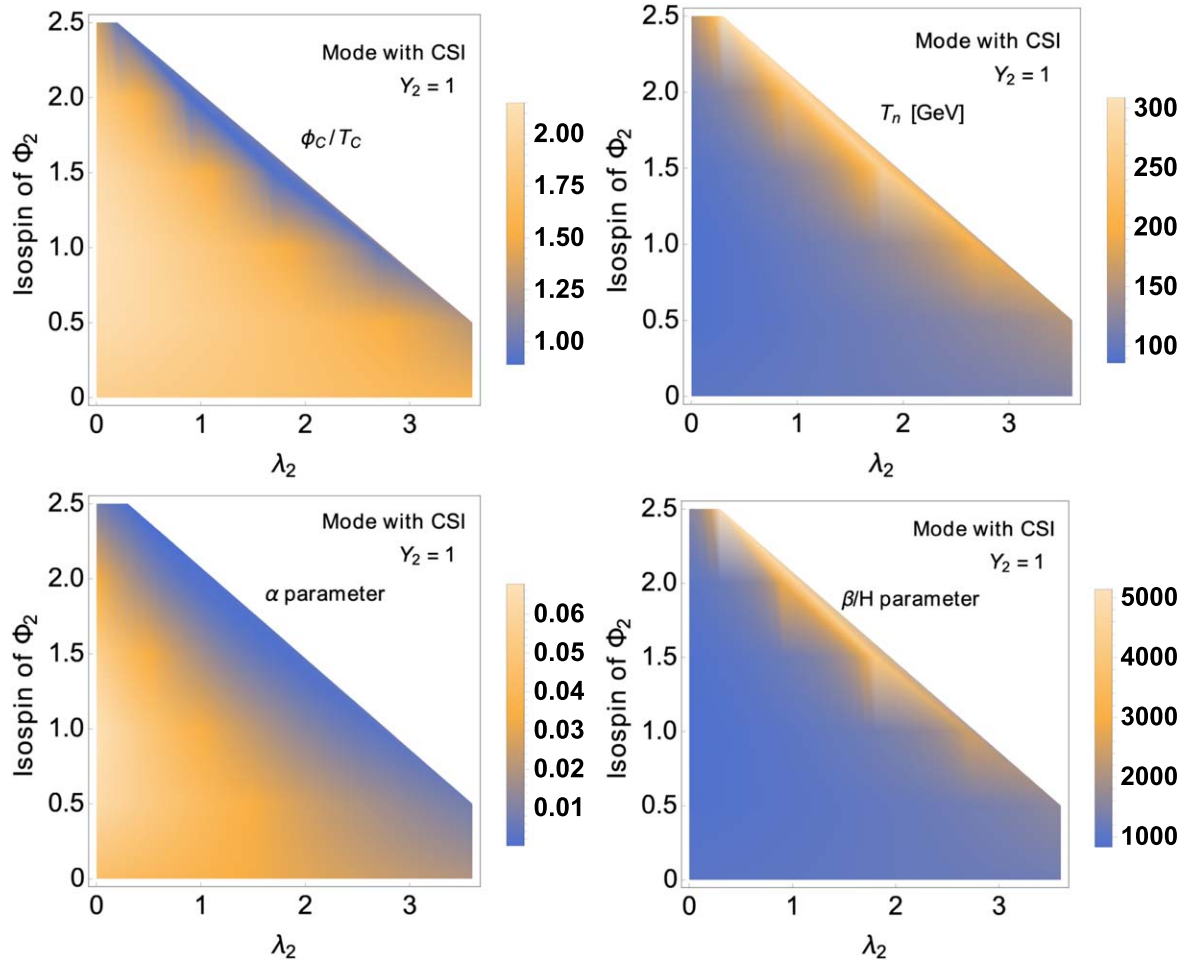

Figure 4. The values of ϕ_C/T_C, T_n, α and β/H for model I with respect to λ_2 coupling and isospin I_{Φ_2} of the additional scalar boson fields.

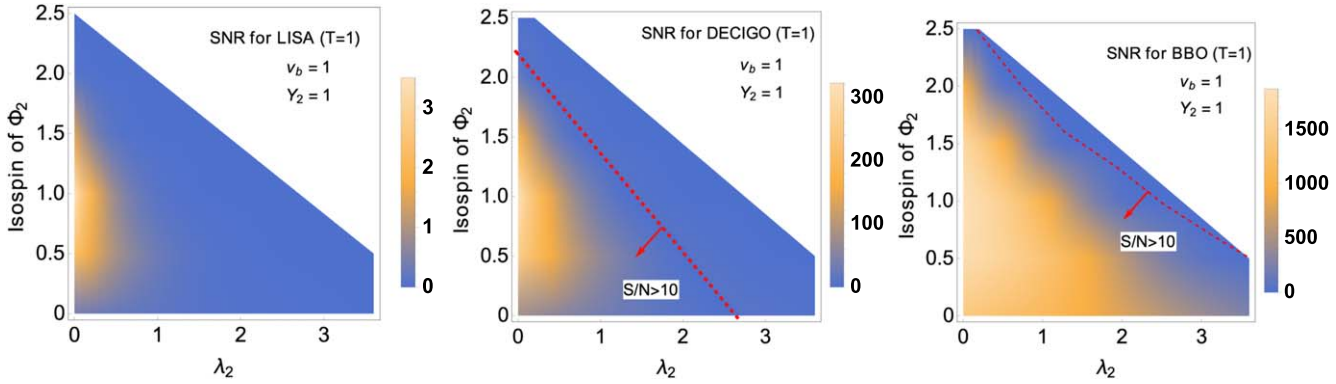

Figure 5. The values of SNR for the model with CSI at LISA, DECIGO and BBO. The experimental period is one year and bubble wall velocity is 1. The red dashed line represents SNR=10.

the Big Bang Observer (BBO). When evaluating the SNR, we simply take the mission duration to be one year and the bubble wall velocity to be one. The red dashed curves in the panels of DECIGO and BBO represent SNR=10. In the parameter regions to the left of the red dashed curves, the SNR is larger than 10, therefore, these parameter regions could be tested at future GW detectors DECIGO and BBO. From these figures, most of parameter regions for the model with CSI could be tested by the DECIGO and BBO missions.

5.2. The model without classical scale invariance

In this section, we show the results for model II, which admits two more free parameters than model I, namely, m_{Φ_2} and λ_{12}. To compare with model I/III with only one-step PT (the additional VEV does not appear in the potential at zero temperature), we will focus on the parameter regions where the same one-step PT for model II as model I/III (green $\rightarrow$ red in figure 2) can be realized. We also neglect the parameter regions with other paths

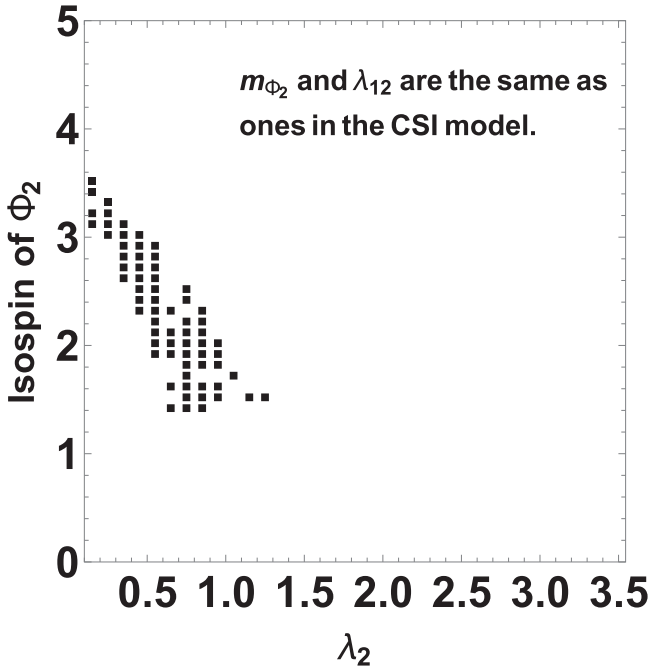

Figure 6. The parameter region can have a stable minimum point along φ_1 and φ_2 axes. At these black points, there is global minimum along φ_2 axis.

of PT, for example, two-step PT (namely the path along green → magenta → red, where the red is a global minimum). We numerically examine the parameter regions where one-step EWPT can be generated by using following four parameter regions: (i) the same m_{Φ_2} and λ_{12} as the model I, (ii) the same m_{Φ_2} as model I, (iii) the same m_{Φ_2} as model III, and (iv) different m_{Φ_2} and λ_{12} from other models.

In parameter region (i), there are the minimum points along φ_1 and φ_2 axes at the black-point region in figure 6, but the minimum points along φ_1 and φ_2 axis are local and global minima, respectively. According to our numerical results, the two-step PT (green → red → magenta) is generated at the black-point region, and the magenta point becomes the true vacuum. In such a case, we cannot explain the fermion mass since the additional scalar field Φ_2 does not couple to the fermion fields anymore. Therefore, in parameter (i) for model II, we cannot realize a proper PT which can make up the current universe. Although model I can generate the detectable GW from the one-step EWPT in figure 5, model II cannot realize the correct PT between green and red points in parameter region (i), which shares the same parameter values as model I. Therefore, we can distinguish the models with and without CSI by the GW detection.

In parameter case (ii), model II admits the same m_{Φ_2} given by equation (27) as model I but with $\lambda_{12} = 1.5$, 2.0, 2.5, 3.0 decoupled from I_{Φ_2} by equation (29) as shown in figure 7, respectively. Note that in the case of model I, m_{Φ_2} and λ_{12} are related by $m_{\Phi_2}^2 = \lambda_{12} v^2/2$, and thus we can get almost the same results for a similar case with the same λ_{12} as model I by equation (29) but decoupled m_{Φ_2} from I_{Φ_2} by equation (27). All colored points in figure 7 admit their global minimum along φ_1 (namely the red point in figure 2).

To show the parameter region where one-step PT along φ_1 axis can be generated, we compare the critical temperatures for the PT along φ_1 and φ_2 axes. From the numerical results, the blue points in figure 7 have a higher critical temperature for the PTs along φ_2 than the PT for φ_1. On the other hand, the green and red points in figure 7 can realize the one-step PT (green → red in figure 2), especially, the red points can realize the strong FOPT along φ_1 axis where the detectable GWs may be generated. At these red points in the model with $\lambda_{12} = 2$ and 2.5, the SNR for BBO with mission time $\mathcal{T}=1$ yr and $v_b = 1$ is larger than 10. Furthermore, the SNR for DECIGO with mission time $\mathcal{T}=1$ yr and $v_b = 1$ at $(\lambda_2, I_{\Phi_2})=(0.25,0.5)$ is about 10.87, while other red points have their SNR no more than 10 for DECIGO. In short summary, a small λ_2 is necessary for detectable GWs in the model II, which is not necessary for model I as shown in figure 5.

To compare the results between model II and model III, we show the results in parameter region (iii) with heavy m_{Φ_2} as model III. For example, the results for heavy $m_{\Phi_2} = 650$ GeV with some λ_2 values in model II are shown in figure 8, however, the effects from the additional heavy scalar field decouple. From the additional scalar mass $M_{\Phi_2}(\varphi)^2 \sim -\mu_2^2 + \lambda_{12}\varphi^2$ with large μ_2^2 value, the cubic term of field-dependent mass in the effective potential can be expanded like $(M_{\Phi_2}^2)^{3/2} \sim |\mu_2^3| + \lambda_{12}\mu_2\varphi^2 + \lambda_{12}^2\varphi^4/\mu_2$, but the cubic φ^3 term does not appear in the potential. On the other hand, the $M_{\Phi_2}(\varphi)^{3/2}$ with small μ_2^2 value can have $\lambda_{12}^{3/2}\varphi^3$ as the source of a barrier. Therefore, it is difficult to generate a sizable barrier to realize first-order EWPT in model II with a much heavier additional scalar field. For the large negative μ_2^2 term, the one-step PT occurs between green and red points in figure 2. In this case, λ_2, which is the coefficient of Φ_2^4, does not much affect the EWPT, and the results are not very different between two figures of figure 8.

The first two panels in figure 9 represent the results in the model with $\lambda_{12}=3$ and $m_{\Phi_2} = 650$ and 425 GeV, which correspond to the parameter regions (iii) and (iv), respectively. With these parameters, the mass parameter μ_2 becomes small (non-decoupling) and the detectable GW spectrum can be generated. Especially, in the model with $m_{\Phi_2}= 425$ GeV, the red (magenta) marks can be described in the upper right figure, and the SNR for DECIGO (BBO) is larger than 10. The last panel in figure 9 represents the results with respect to I_{Φ_2} and m_{Φ_2}, which are related to parameter region (iv) in the model with benchmark parameters $\lambda_2 = 0.5$ and $\lambda_{12} = 2.5$. The blue marks in this model can realize two-step PT. To summarize in short, the detectable GWs, which are represented by the red and magenta marks, can be produced in the massive model with small isospin of Φ_2 and small λ_2 value. However, for model II, such parameter regions with detectable GWs are not the same as those in model I and model III. Therefore we may distinguish the three types of models by the GW observations.

5.3. The model with dimension-six operator from Φ_2

In this section, we discuss the testability for model III. At first, the parameter region of a_6 is shown in figure 10 for detectable

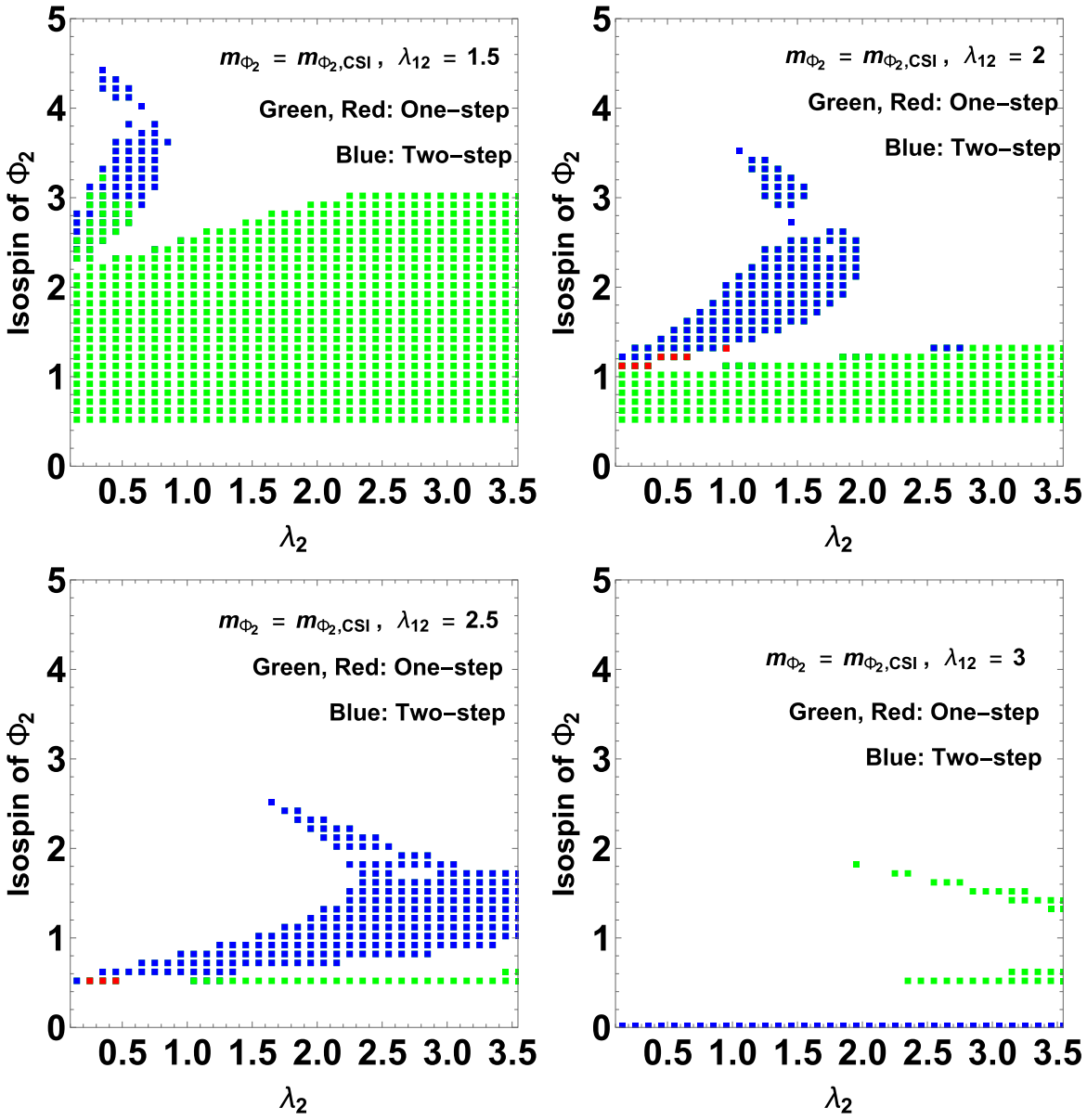

Figure 7. Different PT regions in the parameter space supported by λ_2 and Φ_2 for model II with the same m_{Φ_2} as model I but allowing for different $\lambda_{12} = 1.5, 2.0, 2.5, 3.0$. The blue points represent the two-step PT. The red and green points represent the one-step PT. The detectable GWs at the BBO detection can be generated for the red points. For the rest of the regions in this figure, the global minimum point does not appear along φ_1 axis otherwise the potential is unstable.

GWs at DECIGO and BBO with mission duration $\mathcal{T} = 1$ yr and $v_b = 1$. In the dark regions, the SNR is smaller than 10, hence we require a large a_6 value. Recall that with equation (16), $a_6 = (1 + 2I_{\Phi_2})\frac{1}{(4\pi)^2 m_{\Phi_2}^2}\left(\frac{\lambda_{12}^3}{8} + \frac{\lambda_{12}^2\lambda_1}{6}\right)$, a large a_6 value generally prefers a large isospin I_{Φ_2}, namely a large number of the additional scalar boson fields. We should further check the conditions for a valid EFT expansion $|a_8|v^2/a_6 < 1$ and $2c_{\mathrm{kin}}v^2 < 1/2$, which was discussed in [248]. In this model III, these conditions are

$$\frac{\lambda_{12}v^2}{2m_{\Phi_2}^2} < 1, \quad (1 + 2I_{\Phi_2})\frac{\lambda_{12}^2 v^2}{12(4\pi)^2 m_{\Phi_2}^2} < 1. \tag{82}$$

The left and right panels of figure 11 represent the values of the right hand side of these conditions. The left panel is the comparison between dimension 6 and 8 operators. Since the operators have one-loop level effects, the isospin I_{Φ_2} cancels in this relation. On the other hand, the right panel is the comparison between the tree-level and one-loop level, therefore the value of this relation depends on the isospin I_{Φ_2}. For the presented parameter space, the conditions for a valid EFT expansion can be satisfied.

The values of ϕ_C/T_C, T_n, α and β/H are then shown in figure 12 and the corresponding SNR at DECIGO and BBO are shown in figure 13, where the parameter regions to the right of the red dashed lines have their SNR larger than 10. However, SNR is less than 10^{-5} for LISA, hence LISA may be difficult to test the parameter region of the model III. For detectable GWs from the model III, we require a large number of additional scalar fields (namely a large isospin I_{Φ_2}) and

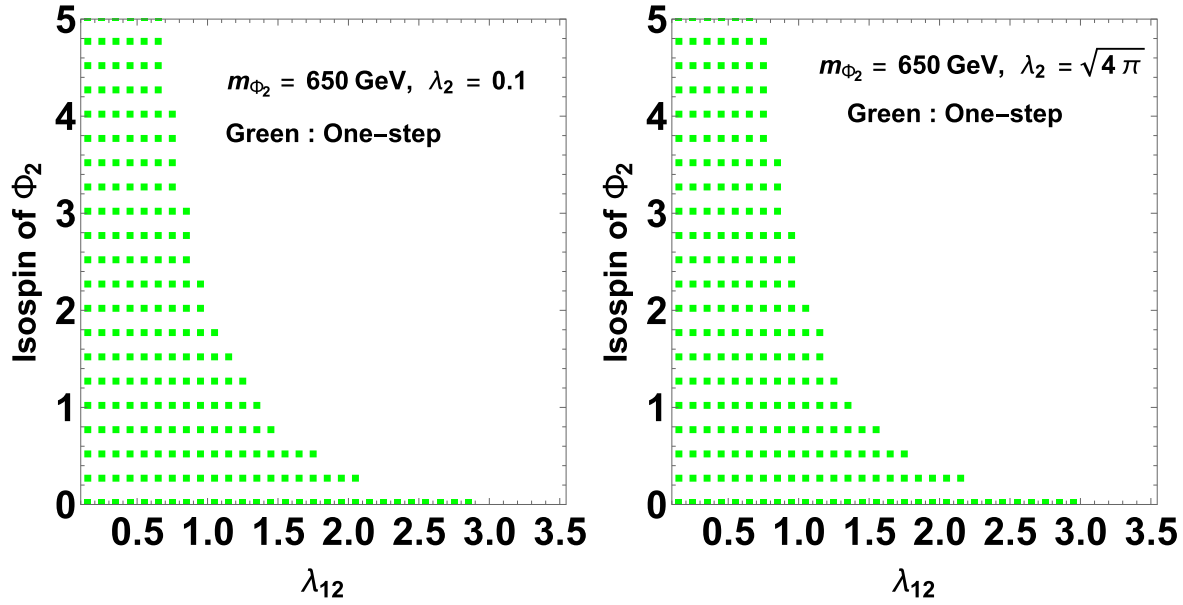

Figure 8. The model parameters for model II with $\lambda_2 = 0.1$, $\sqrt{4\pi}$ and $m_{\Phi_2} = 650$ GeV. The horizontal axis in left and right figures is λ_{12}. Otherwise, the same as figure 7.

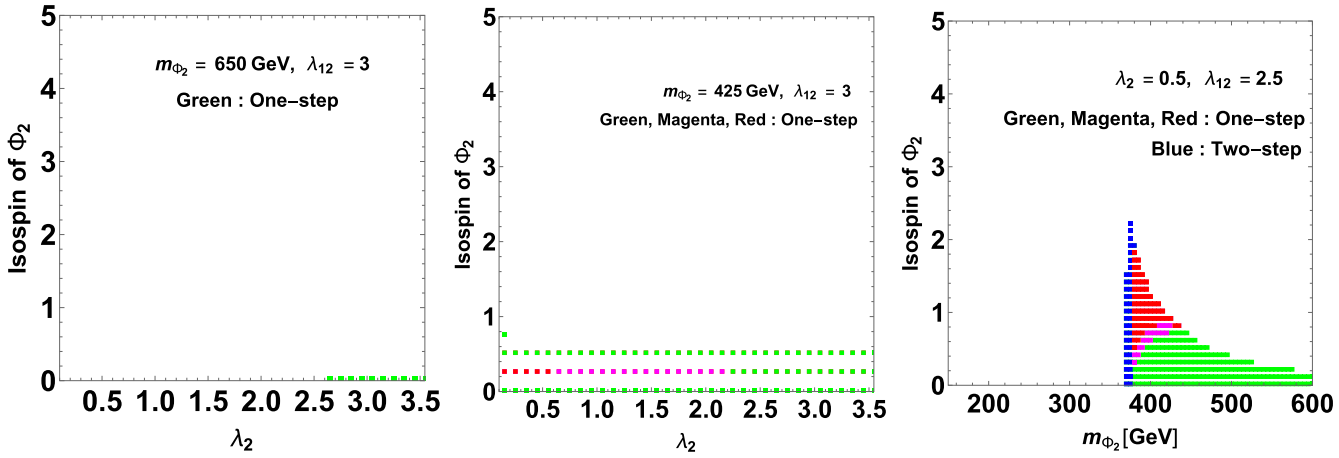

Figure 9. (First two panels) The model parameters for model II with $\lambda_{12} = 3$ and $m_{\Phi_2} = 650$, 425 GeV in the upper left and upper right panels, respectively. At the red (magenta) marks, the detectable GWs at DECIGO (BBO) can be generated. Otherwise, the same as figure 7. (Last panel) The results in the model with $\lambda_2 = 0.5$ and $\lambda_{12} = 2.5$. The horizontal axis is the additional scalar boson mass. The two-step PT occurs at blue marks.

large coupling λ_{12}, which can be distinguished from models I and II by detectable GWs in the parameter regions of small isospin I_{Φ_2}. In particular, model I cannot take the heavy scalar field with $m_{\Phi_2} = 650$ GeV since the additional scalar mass should be less than 543 GeV from equation (27) [267]. Therefore, we may distinguish model III from model I and model II by constraining the isospin of additional scalar fields with the GWs background observed at future GW detectors.

6. Conclusions and discussions

The predictions for the GW background vary sensitively among different concrete models but also share a large degeneracy in the model buildings. From that, in this time, we take into account an EFT treatment for three BSM models based on different patterns of the EWSB: (I) classical scale invariance, (II) generic scalar extension, and (III) higher-dimensional operators. In these EFTs, the EWSB can be realized by (I) radiative symmetry breaking, (II) Higgs mechanism, and (III) EFT description of EWSB, respectively.

These three models can realize the strongly first-order EWPT and can produce the detectable GW spectrum by the effects summarized in Table 2. Here, C_n are the effective couplings of the order parameter operators ϕ^n in the effective potential. The dominant contributions of λ_2 and I_{Φ_2} in models (I) and (II) show up through the ring diagram effects as shown in equations (31), (34), (45) and (47). Thus, a small λ_2 and a small I_{Φ_2} are required to produce the detectable GW spectrum. The differences between models (I) and (II) are the C_2 and C_4 terms and the number of free parameters in the model. In model (II), these terms have tree-level contribution, and thus

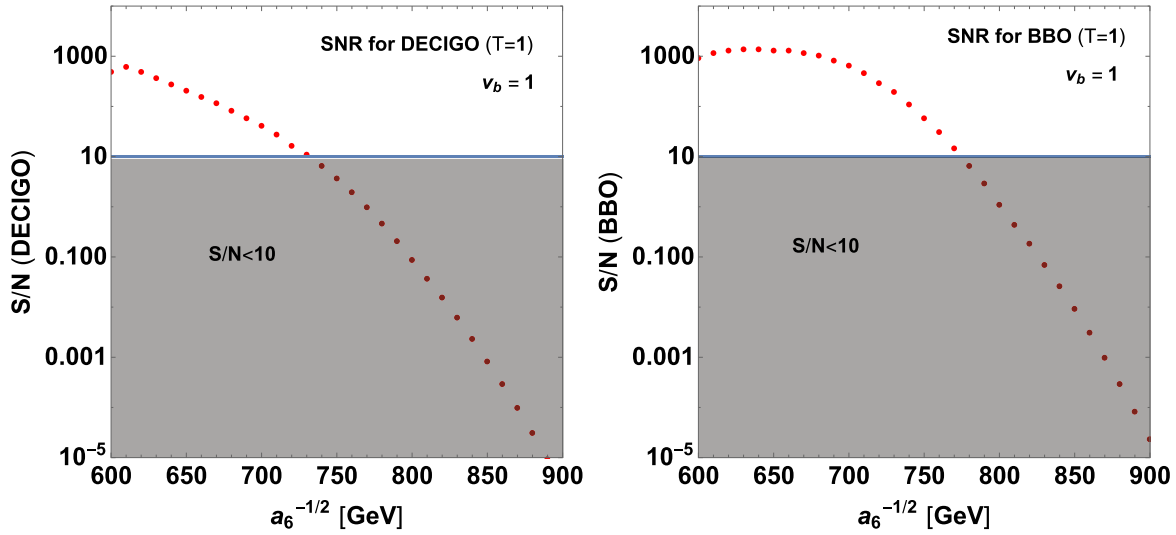

Figure 10. The SNR value from the model with a higher-dimensional operator for DECIGO and BBO with mission year $\mathcal{T} = 1$ yr and $v_b = 1$.

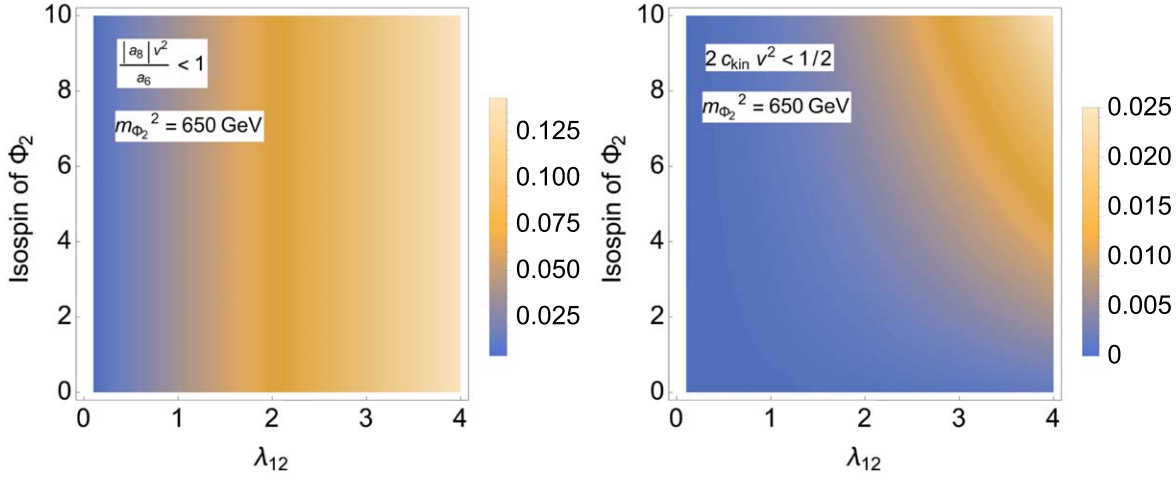

Figure 11. The valid EFT expansion $2c_{\rm kin}v^2 < 1/2$ and $|a_8|v^2/a_6 < 1$ in the model with a higher-dimensional operator with respect to I_{Φ_2} and λ_{12} and fixed $m_{\Phi_2} = 650$ GeV. Since the first condition comes from the comparison between one-loop dimension six and eight operators, the values do not depend on the isospin I_{Φ_2}. For the presented parameter regions, the conditions for a valid EFT expansion can be satisfied.

we need to tune model parameters to have a sizable C_3 comparable with these C_2 and C_4 terms. Unlike model (I), we can use the λ_{12} parameter to realize such a situation and could generate the first-order EWPT as shown in figure 7. On the other hand, the λ_2 in model (III) does not contribute to the effective potential after integrating out the Φ_2 scalar field, and the high dimensional operator $a_6^{-1/2}$ in figure 10 is inversely proportional to λ_{12} and I_{Φ_2} as shown in equation (16). Therefore, a small $a_6^{-1/2}$ can be realized by a large λ_{12} and a large I_{Φ_2}.

These three types of models might be distinguished by investigating the detectable GWs in the parameter regions with overlapping parameters: (1) model I and model II might be distinguished by the detection of GWs in the parameter regions as shown in figures 5 and 6. When taking the same m_{Φ_2} and λ_{12} as model I by equations (27) and (29), model II cannot generate the correct one-step PT where the red point in figure 2 is the local minimum. However, when just taking the same m_{Φ_2} as model I by equation (27) but decoupling λ_{12} from I_{Φ_2} by equation (29), model II could produce detectable GWs in the parameter regions of small λ_2 and small I_{Φ_2}, which is partially overlapping with model I with detectable GWs. In this case, although we cannot fully distinguish models I and II by the GW detections alone, we may use other

Table 2. The potential forms in the three types of the models where the EWSB can be realized by (I) radiative symmetry breaking, (II) Higgs mechanism and (III) EFT description of EWSB, respectively. The last column shows the source of detectable GW spectrum in these models. Otherwise, the same as Table 1.

Model	$C_2\phi^2$	$C_3\phi^3$	$C_4\phi^4$	$C_6\phi^6$	GW features
I	Loop	Loop	Loop	None	Small λ_2 and small I_{Φ_2}
II	Tree	Loop	Tree	None	Small λ_2 and small I_{Φ_2}
III	Tree	Loop	Tree	Tree	Large λ_{12} and large I_{Φ_2}

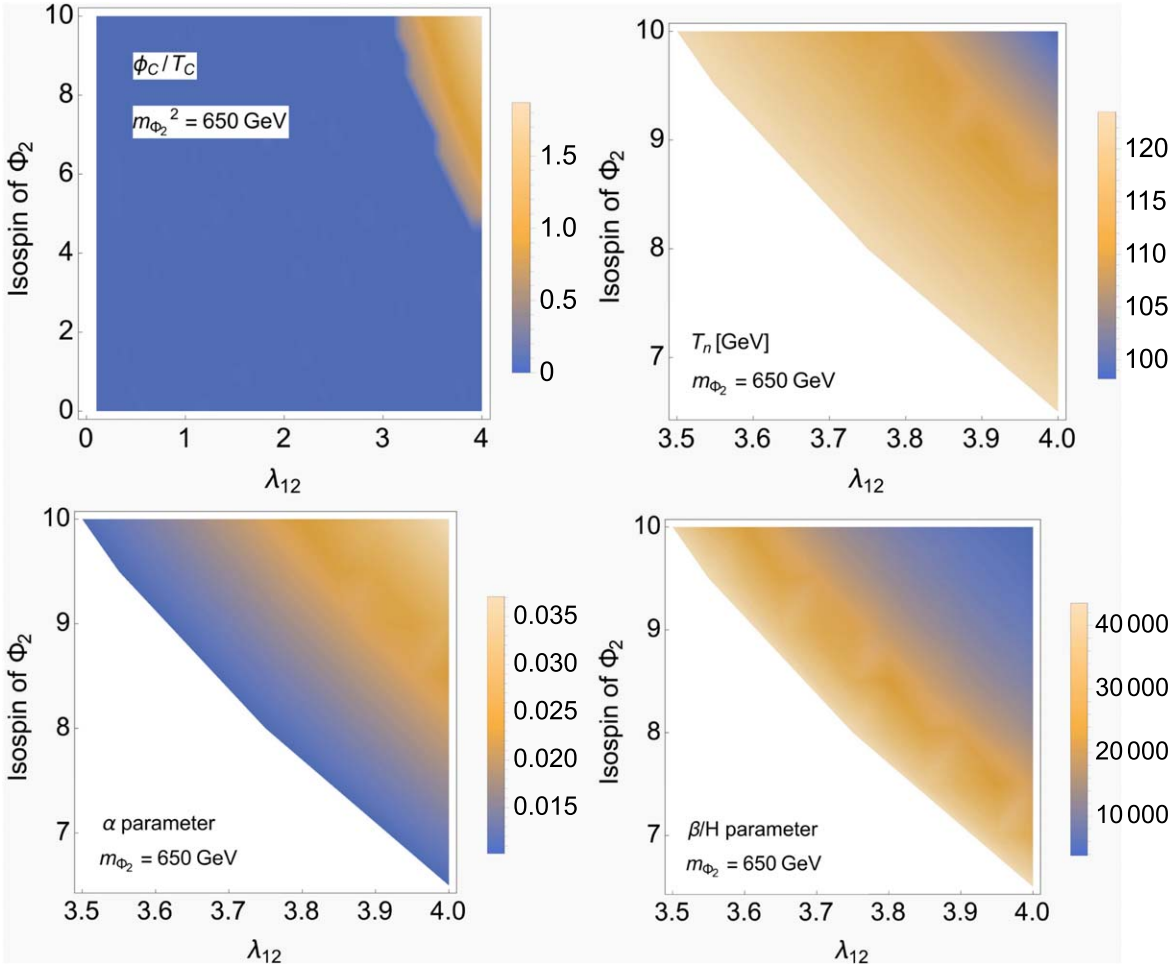

Figure 12. The value of ϕ_C/T_C, T_n, α and β/H in the EFT model with $m_{\Phi_2} = 650$ GeV. Otherwise, the same as figure 11.

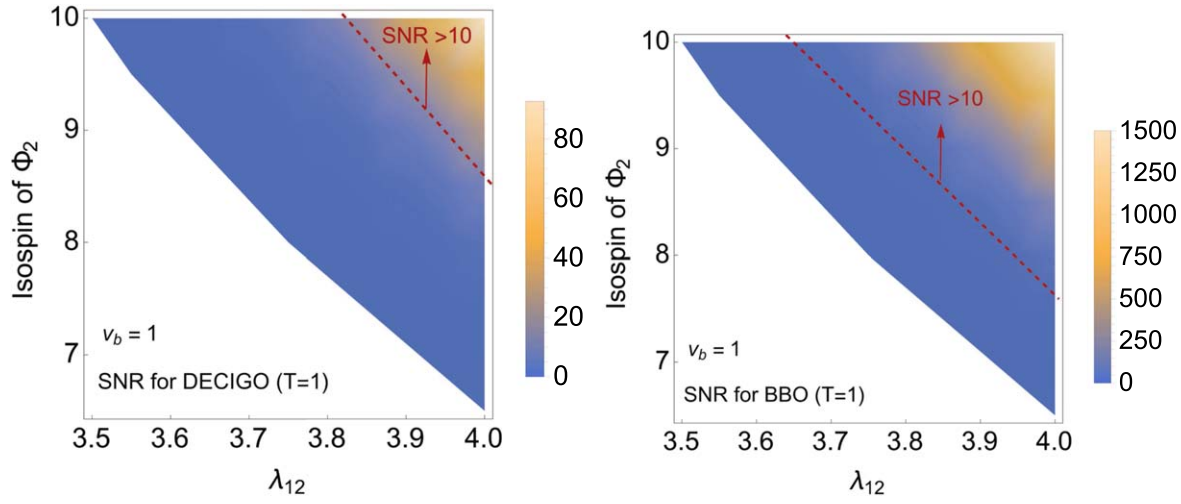

Figure 13. The values of SNR in the EFT model with $m_{\Phi_2} = 650$ GeV at DECIGO and BBO. The ratio of SNR is larger than 10 in the parameter region to right of the red dashed lines.

observations, such as *hhh* coupling [172] and $h\gamma\gamma$ coupling [262, 267], to do that. (2) Model II and model III can be distinguished by the detection of GWs in the parameter regions as shown in figures 8 and 13 since detectable GWs are produced for model II in the parameter regions of small λ_2 and small I_{Φ_2}, while model III favors a large I_{Φ_2} to generate detectable GWs. (3) Similarly, model I could also be distinguished from model III by detectable GWs in the parameter

regions of small I_{Φ_2} (model I) and large I_{Φ_2} (model III). Furthermore, the additional scalar mass should be less than 543 GeV in the model I, different from the case of model III with a heavy scalar field.

Therefore, we may distinguish these three effective model descriptions of EWPT by future GW detections in space. Nevertheless, our PT analysis for the effective model descriptions is preliminary in surveying part of the parameter space, and it only depicts those scalar extensions (with Z_2 symmetry) of fundamental Higgs models [288–290] and Coleman–Weinberg Higgs models [267, 291, 292], but by no means covers all the effective models of EWPT. We will investigate the PT dynamics in a more general classifications of EWSB [293] in the ever-enlarging parameter space in future works.

Acknowledgments

This work is mainly supported by the National Key Research and Development Program of China under Grant Nos. 2021YFC2203004, 2021YFA0718304, and 2020YFC2201501. RGC is supported by the National Natural Science Foundation of China under Grants Nos. 11947302, 11991052, 11690022, 11821505 and 11851302, the Strategic Priority Research Program of the Chinese Academy of Sciences (CAS) under Grant Nos. XDB23030100 and XDA15020701, the Key Research Program of the CAS under Grant No. XDPB15, and the Key Research Program of Frontier Sciences of CAS. SJW is supported by the National Key Research and Development Program of China under Grant Nos. 2021YFC2203004 and 2021YFA0718304, the National Natural Science Foundation of China under Grant Nos. 12422502 and 12105344, the China Manned Space Project under Grant No. CMS-CSST-2021-B01. JHY is supported by the National Science Foundation of China under Grant Nos. 12022514, 11875003 and 12047503, and the National Key Research and Development Program of China under Grant Nos. 2020YFC2201501 and 2021YFA0718304, and the CAS Project for Young Scientists in Basic Research under Grant No. YSBR-006, and the Key Research Program of the CAS under Grant No. XDPB15.

Appendix A Stationary condition and CP-even boson masses in the model without CSI

We use the stationary condition at $(\varphi_1, \varphi_2) = (v, 0)$ and the second derivatives of the potential with one-loop effects,

$$\left.\frac{\partial V_{\rm eff}}{\partial\langle\Phi_1\rangle}\right|_{\langle\Phi_1\rangle=v,\langle\Phi_2\rangle=0}=0,\quad \left.\frac{\partial^2 V_{\rm eff}}{\partial\langle\Phi_1\rangle^2}\right|_{\langle\Phi_1\rangle=v,\langle\Phi_2\rangle=0}=m_h^2, \tag{A1}$$

where we take $Q = v = 246$ GeV. With tadpole condition $\mathcal{M}^2_{\Phi_2\Phi_2} > \mathcal{M}^2_{\Phi_1\Phi_1}$, one arrives at

$$\begin{aligned}\left.\frac{\partial V_{\rm eff}}{\partial\langle\Phi_1\rangle}\right|_{\langle\Phi_1\rangle=v,\langle\Phi_2\rangle=0} &= -\mu_1^2+\lambda_1 v^2+\frac{1}{16\pi^2}\\ &\times\Big[\frac{6\lambda_1+\lambda_{12}}{4}f_+(m^2_{\Phi_{1,r}},m^2_{\Phi_{2,r}})\\ &+\frac{1}{4}(6\lambda_1-\lambda_{12})f_-(m^2_{\Phi_{1,r}},m^2_{\Phi_{2,r}})\\ &+(2(2I_{\Phi_2}-1)-1)\frac{\lambda_{12}m^2_{N_{2,r}}}{2}\\ &\times\left(\ln\frac{m^2_{N_{2,r}}}{Q^2}-1\right)+\frac{6m_W^4}{v^2}\left(\ln\frac{m_W^2}{Q^2}-\frac{1}{3}\right)\\ &+\frac{3m_Z^4}{v^2}\left(\ln\frac{m_Z^2}{Q^2}-\frac{1}{3}\right)\\ &-\frac{12m_t^4}{v^2}\left(\ln\frac{m_t^2}{Q^2}-1\right)\Big]=0,\end{aligned} \tag{A2}$$

where

$$f_\pm(m_i^2,m_j^2)=m_i^2\left(\ln\frac{m_i^2}{Q^2}-1\right)\pm m_j^2\left(\ln\frac{m_j^2}{Q^2}-1\right), \tag{A3}$$

$$\Delta m^2_\Phi=m^2_{\Phi_2}-m^2_{\Phi_1}=\sqrt{(\mathcal{M}^2_{\Phi_1\Phi_1}-\mathcal{M}^2_{\Phi_2\Phi_2})^2+4\mathcal{M}^4_{\Phi_1\Phi_2}}, \tag{A4}$$

$$\mathcal{M}^2_{\text{neutral Higgs}}=\begin{pmatrix}\mathcal{M}^2_{\Phi_1\Phi_1} & \mathcal{M}^2_{\Phi_1\Phi_2}\\ \mathcal{M}^2_{\Phi_2\Phi_1} & \mathcal{M}^2_{\Phi_2\Phi_2}\end{pmatrix} \tag{A5}$$

and the masses in the tadpole conditions of red point case are

$$m^2_{\Phi_{1,r}}=-\mu_1^2+3\lambda_1 v^2,\quad m^2_{\Phi_{2,r}}=-\mu_2^2+\lambda_{12}v^2/2, \tag{A6}$$

$$m^2_{N_{1,r}}=-\mu_1^2+\lambda_1 v^2,\quad m^2_{N_{2,r}}=-\mu_2^2+\lambda_{12}v^2/2, \tag{A7}$$

with $m^2_{\Phi_2} > m_h^2$. In order to replace two of the input parameters in the potential in terms of the Higgs boson mass m_h and additional neutral CP-even boson mass m_{Φ_2}[9], we use

$$\begin{aligned}\left.\frac{\partial^2 V_{\rm eff}}{\partial\langle\Phi_1\rangle^2}\right|_{\langle\Phi_1\rangle=v,\langle\Phi_2\rangle=0} &= 2\lambda_1 v^2+\frac{v^2}{32\pi^2}\\ &\times\Big[A_2^r\ln\frac{m^2_{\Phi_2}m_h^2}{Q^4}-A_3^r\ln\frac{m_h^2}{m^2_{\Phi_2}}\\ &+4\lambda_{12}^2(2(2I_{\Phi_2}-1)-1)\ln\frac{m^2_{N_{2,r}}}{Q^2}\\ &+12\frac{m_Z^4}{v^4}\left(\ln\frac{m_Z^2}{Q^2}+\frac{2}{3}\right)\\ &+24\frac{m_W^4}{v^4}\left(\ln\frac{m_W^2}{Q^2}+\frac{2}{3}\right)-48\frac{m_t^4}{v^4}\ln\frac{m_t^2}{Q^2}\Big]\\ &\equiv m_h^2\end{aligned} \tag{A8}$$

[9] For simplicity, we ignore the contribution from the two-point-function Π_{hh} of the Higgs boson.

$$\left.\frac{\partial^2 V_{\rm eff}}{\partial\langle\Phi_2\rangle^2}\right|_{\langle\Phi_1\rangle=v,\langle\Phi_2\rangle=0} = -\mu_2^2 + \lambda_{12}v^2 + \frac{1}{64\pi^2}[B_1 f_-(m_{\Phi_2}^2, m_h^2) + B_2 f_+(m_{\Phi_2}^2, m_h^2) + 4(2(2I_{\Phi_2} - 1) - 1)\lambda_2 m_{N_{2,r}}^2 \times\left(\ln\frac{m_{N_{2,r}}^2}{Q^2} - 1\right) + 12\frac{m_Z^4 Y_{\Phi_2}^2}{v^2}\left(\ln\frac{m_Z^2}{Q^2} - \frac{1}{3}\right) + 24\frac{m_W^4 I_W^2}{v^2}\left(\ln\frac{m_W^2}{Q^2} - \frac{1}{3}\right)] \equiv m_{\Phi_2}^2, \tag{A9}$$

where

$$A_2^r = \frac{1}{4}((6\lambda_1 + \lambda_{12})^2 + (6\lambda_1 - \lambda_{12})^2), \tag{A10}$$

$$A_3^r = -\frac{36\lambda_1^2 - \lambda_{12}^2}{2}, \tag{A11}$$

$$B_1 = \frac{2}{\Delta m^2}[(-6\lambda_2 + \lambda_{12})(\mathcal{M}_{\Phi_1\Phi_1}^2 - \mathcal{M}_{\Phi_2\Phi_2}^2) + 4\lambda_{12}^2 v^2], \tag{A12}$$

$$B_2 = 6\lambda_2 + \lambda_{12}. \tag{A13}$$

By using equations (A2), (A8) and (A9), we can replace the model parameters:

$$(\mu_1^2, \mu_2^2, \lambda_1, \lambda_2, \lambda_{12}) \to (v, m_{\Phi_2}^2, m_h, \lambda_2, \lambda_{12}). \tag{A14}$$

Appendix B Landau pole in the model with CSI

In this section, we show the Landau pole in the model with CSI. The model with CSI typically has the large values of couplings, which can be obtained by equation (29). The results of the Landau pole is given by figure 14. According to figures 5 and 14, the parameter region with detectable GW spectrum has Landau pole, which is O(1 TeV). When the value of λ_2 will be large, the Landau pole also will be small.

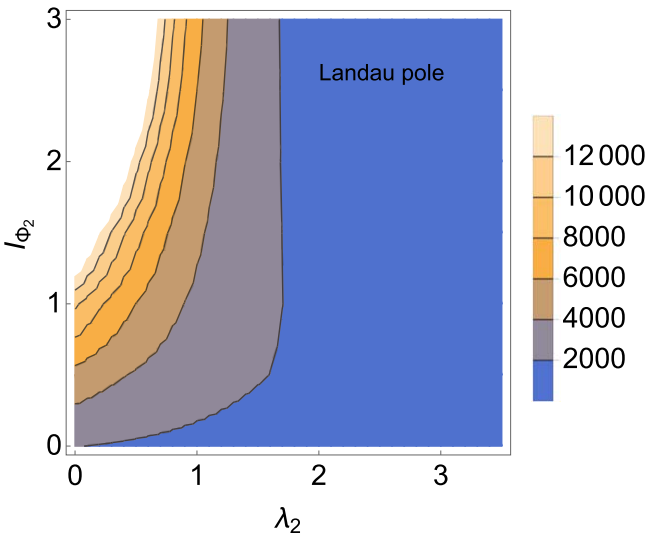

Figure 14. The values of the Landau pole in the CSI model.

References

[1] Zyla P A *et al* (Particle Data Group) 2020 Review of Particle Physics *PTEP* **2020** 083C01

[2] Mazumdar A and White G 2019 Review of cosmic phase transitions: their significance and experimental signatures *Rept. Prog. Phys.* **82** 076901

[3] Hindmarsh M B, Lüben M, Lumma J and Pauly M 2021 Phase transitions in the early universe *SciPost Phys. Lect. Notes* **24** 1

[4] Caprini C *et al* 2016 Science with the space-based interferometer eLISA. II: Gravitational waves from cosmological phase transitions *J. Cosmol. Astropart. Phys.* **2016** JCAP04(2016)001

[5] Caprini C *et al* 2020 Detecting gravitational waves from cosmological phase transitions with LISA: an update *J. Cosmol. Astropart. Phys.* **2020** JCAP03(2020)024

[6] Amaro-Seoane P *et al* 2017 Laser interferometer space antenna arXiv:1702.00786

[7] Binetruy P, Bohe A, Caprini C and Dufaux J-F 2012 Cosmological backgrounds of gravitational waves and eLISA/NGO: Phase transitions, cosmic strings and other sources *J. Cosmol. Astropart. Phys.* **2012** JCAP06(2012)027

[8] Amaro-Seoane P *et al* 2012 Low-frequency gravitational-wave science with eLISA/NGO *Class. Quantum Grav.* **29** 124016

[9] Amaro-Seoane P *et al* 2013 eLISA/NGO: Astrophysics and cosmology in the gravitational-wave millihertz regime arXiv:1201.3621

[10] Weir D J 2018 Gravitational waves from a first order electroweak phase transition: a brief review *Phil. Trans. Roy. Soc. Lond* **A376** 20170126

[11] Figueroa D G, Megias E, Nardini G, Pieroni M, Quiros M, Ricciardone A and Tasinato G 2018 LISA as a probe for particle physics: electroweak scale tests in synergy with ground-based experiments *Gravitational-Waves Science & Technology Symposium (GRASS2018)* 036 *(Padova, Italy, March 1-2, 2018)*

[12] Fitz Axen M, Banagiri S, Matas A, Caprini C and Mandic V 2018 Multiwavelength observations of cosmological phase transitions using LISA and Cosmic Explorer *Phys. Rev.* D **98** 103508

[13] Cai R-G, Cao Z, Guo Z-K, Wang S-J and Yang T 2017 The Gravitational-Wave Physics *Natl. Sci. Rev.* **4** 687–706

[14] Bian L *et al* 2021 The Gravitational-wave physics II: Progress *Sci. China Phys. Mech. Astron.* **64** 120401

[15] Kajantie K, Laine M, Rummukainen K and Shaposhnikov M E 1996 Is there a hot electroweak phase transition at $m_H \gtrsim m_W$ *Phys. Rev. Lett.* **77** 2887–90

[16] Zhang X-min 1993 Operators analysis for Higgs potential and cosmological bound on Higgs mass *Phys. Rev.* D **47** 3065–7

[17] Bodeker D, Fromme L, Huber S J and Seniuch M 2005 The Baryon asymmetry in the standard model with a low cut-off *J. High Energy Phys.* **2005** JHEP02(2005)026

[18] Grojean C, Servant G and Wells J D 2005 First-order electroweak phase transition in the standard model with a low cutoff *Phys. Rev.* D **71** 036001

[19] Delaunay C, Grojean C and Wells J D 2008 Dynamics of Non-renormalizable electroweak symmetry breaking *J. High Energy Phys.* **2008** 029

[20] Huber S J and Konstandin T 2008 Production of gravitational waves in the nMSSM *J. Cosmol. Astropart. Phys.* **2008** JCAP05(2008)017

[21] Huber S J and Sopena M 2013 An efficient approach to electroweak bubble velocities arXiv:1302.1044

[22] Konstandin T, Nardini G and Rues I 2014 From Boltzmann equations to steady wall velocities *J. Cosmol. Astropart. Phys.* **2014** JCAP09(2014)028

[23] Damgaard P H, Haarr A, O'Connell D and Tranberg A 2016 Effective field theory and electroweak baryogenesis in the singlet-extended standard model *J. High Energy Phys.* **2016** JHEP02(2016)107

[24] Leitao L and Megevand A 2016 Gravitational waves from a very strong electroweak phase transition *J. Cosmol. Astropart. Phys.* **2016** JCAP05(2016)037

[25] Harman C P D and Huber S J 2016 Does zero temperature decide on the nature of the electroweak phase transition? *J. High Energy Phys.* **2016** JHEP06(2016)005

[26] Huang F P, Wan Y, Wang D-G, Cai Y-F and Zhang X 2016 Hearing the echoes of electroweak baryogenesis with gravitational wave detectors *Phys. Rev.* D **94** 041702

[27] Balazs C, White G and Yue J 2017 Effective field theory, electric dipole moments and electroweak baryogenesis *J. High Energy Phys.* **2017** JHEP03(2017)030

[28] de Vries J, Postma M, van de Vis J and White G 2018 Electroweak baryogenesis and the standard model effective field theory *J. High Energy Phys.* **2018** JHEP01(2018)089

[29] Cai R-G, Sasaki M and Wang S-J 2017 The gravitational waves from the first-order phase transition with a dimension-six operator *J. Cosmol. Astropart. Phys.* **2017** JCAP08 (2017)004

[30] Chala M, Krause C and Nardini G 2018 Signals of the electroweak phase transition at colliders and gravitational wave observatories *J. High Energy Phys.* **2018** JHEP07 (2018)062

[31] Dorsch G C, Huber S J and Konstandin T 2018 Bubble wall velocities in the standard model and beyond *J. Cosmol. Astropart. Phys.* **2018** JCAP12(2018)034

[32] Vries J D, Postma M and Vis J D 2019 The role of leptons in electroweak baryogenesis *J. High Energy Phys.* **2019** JHEP04(2019)024

[33] Ellis S A R, Ipek S and White G 2019 Electroweak baryogenesis from temperature-varying couplings *J. High Energy Phys.* **2019** JHEP08(2019)002

[34] Chala M, Khoze V V, Spannowsky M and Waite P 2019 Mapping the shape of the scalar potential with gravitational waves *Int. J. Mod. Phys.* A **34** 1950223

[35] Zhou R, Bian L and Guo H-K 2020 Connecting the electroweak sphaleron with gravitational waves *Phys. Rev.* D **101** 091903

[36] Phong V Q, Khiem P H, Loc N P D and Long H N 2020 Sphaleron in the first-order electroweak phase transition with the dimension-six Higgs field operator *Phys. Rev.* D **101** 116010

[37] Kanemura S and Tanaka M 2020 Higgs boson coupling as a probe of the sphaleron property *Phys. Lett.* B **809** 135711

[38] Hashino K, Kanemura S and Takahashi T 2022 Primordial black holes as a probe of strongly first-order electroweak phase transition *Phys. Lett.* B **833** 137261

[39] Kanemura S and Nagai R 2021 A new Higgs effective field theory and the new no-lose theorem *J. High Energy Phys.* **2022** JHEP03(2022)194

[40] Profumo S, Ramsey-Musolf M J and Shaughnessy G 2007 Singlet Higgs phenomenology and the electroweak phase transition *J. High Energy Phys.* **2007** JHEP08(2007)010

[41] Espinosa J R, Konstandin T and Riva F 2012 Strong electroweak phase transitions in the standard model with a singlet *Nucl. Phys.* B **854** 592–630

[42] Profumo S, Ramsey-Musolf M J, Wainwright C L and Winslow P 2015 Singlet-catalyzed electroweak phase transitions and precision Higgs boson studies *Phys. Rev.* D **91** 035018

[43] Jinno R, Nakayama K and Takimoto M 2016 Gravitational waves from the first order phase transition of the Higgs field at high energy scales *Phys. Rev.* D **93** 045024

[44] Huang P, Long A J and Wang L-T 2016 Probing the electroweak phase transition with higgs factories and gravitational waves *Phys. Rev.* D **94** 075008

[45] Balazs C, Fowlie A, Mazumdar A and White G 2017 Gravitational waves at aLIGO and vacuum stability with a scalar singlet extension of the Standard Model *Phys. Rev.* D **95** 043505

[46] Curtin D, Meade P and Ramani H 2018 Thermal resummation and phase transitions *Eur. Phys. J.* C **78** 787

[47] Hashino K, Kakizaki M, Kanemura S, Ko P and Matsui T 2017 Gravitational waves and Higgs boson couplings for exploring first order phase transition in the model with a singlet scalar field *Phys. Lett.* B **766** 49–54

[48] Vaskonen V 2017 Electroweak baryogenesis and gravitational waves from a real scalar singlet *Phys. Rev.* D **95** 123515

[49] Kurup G and Perelstein M 2017 Dynamics of electroweak phase transition in singlet-scalar extension of the standard model *Phys. Rev.* D **96** 015036

[50] Beniwal A, Lewicki M, Wells J D, White M and Williams A G 2017 Gravitational wave, collider and dark matter signals from a scalar singlet electroweak baryogenesis *J. High Energy Phys.* **2017** 108

[51] Kang Z, Ko P and Matsui T 2018 Strong first order EWPT & strong gravitational waves in Z_3-symmetric singlet scalar extension *J. High Energy Phys.* **2018** 115

[52] Chen C-Y, Kozaczuk J and Lewis I M 2017 Non-resonant collider signatures of a singlet-driven electroweak phase transition *J. High Energy Phys.* **2017** 096

[53] Chao W, Guo H-K and Shu J 2017 Gravitational wave signals of electroweak phase transition triggered by dark matter *J. Cosmol. Astropart. Phys.* **2017** JCAP09(2017)009

[54] Beniwal A, Lewicki M, White M and Williams A G 2019 Gravitational waves and electroweak baryogenesis in a global study of the extended scalar singlet model *J. High Energy Phys.* **2019** 183

[55] Shajiee V R and Tofighi A 2019 Electroweak phase transition, gravitational waves and dark matter in two scalar singlet extension of the standard model *Eur. Phys. J.* C **79** 360

[56] Alves A, Ghosh T, Guo H-K, Sinha K and Vagie D 2019 Collider and gravitational wave complementarity in exploring the singlet extension of the standard model *J. High Energy Phys.* **2019** 052

[57] Grzadkowski B and Huang D 2018 Spontaneous CP-Violating electroweak baryogenesis and dark matter from a complex singlet scalar *J. High Energy Phys.* **2018** 135

[58] Hashino K, Jinno R, Kakizaki M, Kanemura S, Takahashi T and Takimoto M 2019 Selecting models of first-order phase transitions using the synergy between collider and gravitational-wave experiments *Phys. Rev.* D **99** 075011

[59] Ahriche A, Hashino K, Kanemura S and Nasri S 2019 Gravitational waves from phase transitions in models with charged singlets *Phys. Lett.* B **789** 119–26

[60] Imtiaz B, Cai Y-F and Wan Y 2019 Two-field cosmological phase transitions and gravitational waves in the singlet Majoron model *Eur. Phys. J.* C **79** 25

[61] Chen N, Li T, Wu Y and Bian L 2020 Complementarity of the future e^+e^- colliders and gravitational waves in the probe of complex singlet extension to the standard model *Phys. Rev. D* **101** 075047

[62] Alves A, Gonalves D, Ghosh T, Guo H-K and Sinha K 2020 Di-Higgs Production in the 4b Channel and Gravitational Wave Complementarity *J. High Energy Phys.* **03** 053

[63] Kannike K, Loos K and Raidal M 2020 Gravitational wave signals of pseudo-Goldstone dark matter in the $\mathbb{Z}_3$ complex singlet model *Phys. Rev.* D **101** 035001

[64] Chiang C-W and Lu B-Q 2020 First-order electroweak phase transition in a complex singlet model with $\mathbb{Z}_3$ symmetry *J. High Energy Phys.* **2020** 082
[65] Kozaczuk J, Ramsey-Musolf M J and Shelton J 2020 Exotic Higgs boson decays and the electroweak phase transition *Phys. Rev.* D **101** 115035
[66] Carena M, Liu Z and Wang Y 2020 Electroweak phase transition with spontaneous Z_2-breaking *J. High Energy Phys.* **2020** 107
[67] Alves A, Gonçalves D, Ghosh T, Guo H-K and Sinha K 2021 Di-higgs blind spots in gravitational wave signals *Phys. Lett.* B **818** 136377
[68] Bari P D, Marfatia D and Zhou Y-L 2020 Gravitational waves from neutrino mass and dark matter genesis *Phys. Rev.* D **102** 095017
[69] Pandey M and Paul A 2020 Gravitational wave emissions from first order phase transitions with two component fimp dark matter arXiv:2003.08828
[70] Alanne T, Benincasa N, Heikinheimo M, Kannike K, Keus V, Koivunen N and Tuominen K 2020 Pseudo-Goldstone dark matter: gravitational waves and direct-detection blind spots *J. High Energy Phys.* **2020** 080
[71] Paul A, Mukhopadhyay U and Majumdar D 2021 Gravitational wave signatures from domain wall and strong first-order phase transitions in a two complex scalar extension of the Standard Model *J. High Energy Phys.* **2021** 223
[72] Xie K-P 2021 Lepton-mediated electroweak baryogenesis, gravitational waves and the 4τ final state at the collider *J. High Energy Phys.* **2021** 090
[73] Kanemura S and Tanaka M 2022 Strongly first-order electroweak phase transition by relatively heavy additional Higgs bosons *Phys. Rev.* D **106** 035012
[74] Huet P and Nelson A E 1995 CP violation and electroweak baryogenesis in extensions of the standard model *Phys. Lett.* B **355** 229–35
[75] Cline J M and Lemieux P-A 1997 Electroweak phase transition in two Higgs doublet models *Phys. Rev.* D **55** 3873–81
[76] Fromme L, Huber S J and Seniuch M 2006 Baryogenesis in the two-Higgs doublet model *J. High Energy Phys.* **2006** JHEP11(2006)038
[77] Cline J M, Kainulainen K and Trott M 2011 Electroweak Baryogenesis in Two Higgs Doublet Models and B meson anomalies *J. High Energy Phys.* **2011** 089
[78] Dorsch G C, Huber S J and No J M 2013 A strong electroweak phase transition in the 2HDM after LHC8 *J. High Energy Phys.* **2013** 29
[79] Dorsch G C, Huber S J, Mimasu K and No J M 2014 Echoes of the Electroweak Phase Transition: Discovering a second Higgs doublet through $A_0 \to ZH_0$ *Phys. Rev. Lett.* **113** 211802
[80] Kakizaki M, Kanemura S and Matsui T 2015 Gravitational waves as a probe of extended scalar sectors with the first order electroweak phase transition *Phys. Rev.* D **92** 115007
[81] Dorsch G C, Huber S J, Konstandin T and No J M 2017 A second higgs doublet in the early universe: baryogenesis and gravitational waves *J. Cosmol. Astropart. Phys.* **2017** JCAP05(2017)052
[82] Basler P, Krause M, Muhlleitner M, Wittbrodt J and Wlotzka A 2017 Strong first order electroweak phase transition in the CP-conserving 2HDM revisited *J. High Energy Phys.* **2017** 121
[83] Bernon J, Bian L and Jiang Y 2018 A new insight into the phase transition in the early Universe with two Higgs doublets *J. High Energy Phys.* **2018** 151
[84] Dorsch G C, Huber S J, Mimasu K and No J M 2017 The higgs vacuum uplifted: revisiting the electroweak phase transition with a second higgs doublet *J. High Energy Phys.* **2017** 086
[85] Huang F P and Yu J-H 2018 Exploring inert dark matter blind spots with gravitational wave signatures *Phys. Rev.* D **98** 095022
[86] Basler P, Mhlleitner M and Wittbrodt J 2018 The CP-violating 2HDM in light of a strong first order electroweak phase transition and implications for higgs pair production *J. High Energy Phys.* **2018** 061
[87] Barman B, Dutta Banik A and Paul A 2020 Singlet-doublet fermionic dark matter and gravitational waves in a two-Higgs-doublet extension of the Standard Model *Phys. Rev.* D **101** 055028
[88] Wang X, Huang F P and Zhang X 2020 Gravitational wave and collider signals in complex two-Higgs doublet model with dynamical CP-violation at finite temperature *Phys. Rev.* D **101** 015015
[89] Zhou R and Bian L 2020 Gravitational wave and electroweak baryogenesis with two Higgs doublet models *Phys. Lett.* B **829** 137105
[90] Gonçalves D, Kaladharan A and Wu Y 2021 Electroweak phase transition in the 2HDM: collider and gravitational wave complementarity *Phys. Rev.* D **105** 095041
[91] Gráf Lukáš, Jana S, Kaladharan A and Saad S 2021 Gravitational wave imprints of left-right symmetric model with minimal higgs sector *J. Cosmol. Astropart. Phys.* **2022** JCAP05(2022)003
[92] Patel H H and Ramsey-Musolf M J 2013 Stepping into electroweak symmetry breaking: phase transitions and Higgs phenomenology *Phys. Rev.* D **88** 035013
[93] Inoue S, Ovanesyan G and Ramsey-Musolf M J 2016 Two-step electroweak baryogenesis *Phys. Rev.* D **93** 015013
[94] Blinov N, Kozaczuk J, Morrissey D E and Tamarit C 2015 Electroweak baryogenesis from exotic electroweak symmetry breaking *Phys. Rev.* D **92** 035012
[95] Chala M, Ramos M and Spannowsky M 2019 Gravitational wave and collider probes of a triplet Higgs sector with a low cutoff *Eur. Phys. J.* C **79** 156
[96] Zhou R, Cheng W, Deng X, Bian L and Wu Y 2019 Electroweak phase transition and Higgs phenomenology in the Georgi-Machacek model *J. High Energy Phys.* **2019** 216
[97] Addazi A, Marcian A, Morais A P, Pasechnik R, Srivastava R and Valle J W F 2020 Gravitational footprints of massive neutrinos and lepton number breaking *Phys. Lett.* B **807** 135577
[98] Benincasa N, Kannike K, Hektor A, Hryczuk A and Loos K 2020 Phase transitions and gravitational waves in models of $\mathbb{Z}_N$ scalar dark matter *2019 European Physical Society Conference on High Energy Physics (EPS-HEP2019)* 364 *(Ghent, Belgium)*
[99] Brdar V, Graf L, Helmboldt A J and Xu X-J 2019 Gravitational waves as a probe of left-right symmetry breaking *J. Cosmol. Astropart. Phys.* **2019** JCAP12 (2019)027
[100] Paul A, Banerjee B and Majumdar D 2019 Gravitational wave signatures from an extended inert doublet dark matter model *J. Cosmol. Astropart. Phys.* **2019** JCAP10(2019)062
[101] Bian L, Guo H-K, Wu Y and Zhou R 2020 Gravitational wave and collider searches for electroweak symmetry breaking patterns *Phys. Rev.* D **101** 035011
[102] Niemi L, Ramsey-Musolf M J, Tenkanen T V I and Weir D J 2021 Thermodynamics of a two-step electroweak phase transition *Phys. Rev. Lett.* **126** 171802
[103] Wang Y, Li C S and Huang F P 2021 Complementary probe of dark matter blind spots by lepton colliders and gravitational waves *Phys. Rev.* D **104** 053004
[104] Borah D, Dasgupta A, Fujikura K, Kyu Kang S and Mahanta D 2020 Observable gravitational waves in minimal

scotogenic model *J. Cosmol. Astropart. Phys.* **2008** JCAP08 (2020)046
[105] Grinstein B and Trott M 2008 Electroweak baryogenesis with a pseudo-Goldstone Higgs *Phys. Rev.* D **78** 075022
[106] Panico G, Redi M, Tesi A and Wulzer A 2013 On the tuning and the mass of the composite higgs *J. High Energy Phys.* **2013** 051
[107] Grojean C, Matsedonskyi O and Panico G 2013 Light top partners and precision physics *J. High Energy Phys.* **2013** 160
[108] Csáki C, Geller M and Telem O 2018 Tree-level quartic for a holographic composite higgs *J. High Energy Phys.* **2018** 134
[109] Espinosa J R, Ben G, Thomas K and Francesco R 2012 Electroweak baryogenesis in non-minimal composite higgs models *J. Cosmol. Astropart. Phys.* **2012** JCAP01(2012)012
[110] Bian L, Wu Y and Xie K-P 2019 Electroweak phase transition with composite Higgs models: calculability, gravitational waves and collider searches *J. High Energy Phys.* **2019** 028
[111] De Curtis S, Rose L D and Panico G 2019 Composite dynamics in the early universe *J. High Energy Phys.* **2019** 149
[112] Xie K-P, Bian L and Wu Y 2020 Electroweak baryogenesis and gravitational waves in a composite Higgs model with high dimensional fermion representations *J. High Energy Phys.* **2020** 047
[113] Chala M, Nardini G and Sobolev I 2016 Unified explanation for dark matter and electroweak baryogenesis with direct detection and gravitational wave signatures *Phys. Rev.* D **94** 055006
[114] Fujikura K, Kamada K, Nakai Y and Yamaguchi M 2018 Phase transitions in twin Higgs models *J. High Energy Phys.* **2018** 018
[115] Chala M, Grber R and Spannowsky M 2018 Searches for vector-like quarks at future colliders and implications for composite Higgs models with dark matter *J. High Energy Phys.* **2018** 040
[116] Bruggisser S, Von Harling B, Matsedonskyi O and Servant G 2018 Electroweak phase transition and baryogenesis in composite higgs models *J. High Energy Phys.* **2018** 099
[117] Bruggisser S, Harling B V, Matsedonskyi O and Servant G 2018 Baryon asymmetry from a composite Higgs boson *Phys. Rev. Lett.* **121** 131801
[118] Delepine D, Gerard J M, Gonzalez Felipe R and Weyers J 1996 A light stop and electroweak baryogenesis *Phys. Lett.* B **386** 183–8
[119] Carena M, Quiros M and Wagner C E M 1996 Opening the window for electroweak baryogenesis *Phys. Lett.* B **380** 81–91
[120] Apreda R, Maggiore M, Nicolis A and Riotto A 2001 Supersymmetric phase transitions and gravitational waves at LISA, *Class Quantum Grav.* **18** L155
[121] Laine M, Nardini G and Rummukainen K 2013 Lattice study of an electroweak phase transition at $m_h \simeq 126$ GeV *J. Cosmol. Astropart. Phys.* **2013** JCAP01(2013)011
[122] Leitao L, Megevand A and Sanchez A D 2012 Gravitational waves from the electroweak phase transition *J. Cosmol. Astropart. Phys.* **2012** JCAP10(2012)024
[123] Menon A and Morrissey D E 2009 Higgs boson signatures of MSSM electroweak baryogenesis *Phys. Rev.* D **79** 115020
[124] Curtin D, Jaiswal P and Meade P 2012 Excluding electroweak baryogenesis in the MSSM *J. High Energy Phys.* **2012** 005
[125] Carena M, Nardini G, Quiros M and Wagner C E M 2013 MSSM electroweak baryogenesis and LHC data *J. High Energy Phys.* **02** 001
[126] Cohen T, Morrissey D E and Pierce A 2012 Electroweak baryogenesis and Higgs signatures *Phys. Rev.* D **86** 013009
[127] Liebler S, Profumo S and Stefaniak T 2016 Light stop mass limits from higgs rate measurements in the MSSM: Is MSSM electroweak baryogenesis still alive after all *J. High Energy Phys.* **2016** 143
[128] Katz A, Perelstein M, Ramsey-Musolf M J and Winslow P 2015 Stop-catalyzed baryogenesis beyond the MSSM *Phys. Rev.* D **92** 095019
[129] Pietroni M 1993 The electroweak phase transition in a nonminimal supersymmetric model *Nucl. Phys.* B **402** 27–45
[130] Davies A T, Froggatt C D and Moorhouse R G 1996 Electroweak baryogenesis in the next-to-minimal supersymmetric model *Phys. Lett.* B **372** 88–94
[131] Apreda R, Maggiore M, Nicolis A and Riotto A 2002 Gravitational waves from electroweak phase transitions *Nucl. Phys.* B **631** 342–68
[132] Menon A, Morrissey D E and Wagner C E M 2004 Electroweak baryogenesis and dark matter in the nMSSM *Phys. Rev.* D **70** 035005
[133] Das S, Fox P J, Kumar A and Weiner N 2010 The Dark Side of the Electroweak Phase Transition *J. High Energy Phys.* **2010** 108
[134] Kozaczuk J, Profumo S and Wainwright C L 2013 Electroweak baryogenesis and the fermi gamma-ray line *Phys. Rev.* D **87** 075011
[135] Kozaczuk J, Profumo S, Haskins L S and Wainwright C L 2015 Cosmological phase transitions and their properties in the NMSSM *J. High Energy Phys.* **2015** 144
[136] Huber S J, Konstandin T, Nardini G and Rues I 2016 Detectable gravitational waves from very strong phase transitions in the general NMSSM *J. Cosmol. Astropart. Phys.* **2016** JCAP03(2016)036
[137] Demidov S V, Gorbunov D S and Kirpichnikov D V 2016 Detectable gravitational waves from very strong phase transitions in the general NMSSM *J. Cosmol. Astropart. Phys.* **2016** JCAP03(2016)036
[138] Demidov S V, Gorbunov D S and Kirpichnikov D V 2018 Gravitational waves from phase transition in split NMSSM *Phys. Lett.* B **779** 191–4
[139] Bian L, Guo H-K and Shu J 2018 Gravitational waves, baryon asymmetry of the universe and electric dipole moment in the CP-violating NMSSM *Chin. Phys.* C **42** 093106
Erratum: 2019 *Chin. Phys.* C **43, No.12** 129101
[140] Akula S, Balzs C, Dunn L and White G 2017 Electroweak baryogenesis in the $\mathbb{Z}_3$ -invariant NMSSM *J. High Energy Phys.* **2017** 051
[141] Georgi H and Machacek M 1985 Doubly charged higgs bosons *Nucl. Phys.* B **262** 463–77
[142] Cort L, Garcia M and Quiros M 2013 Supersymmetric custodial triplets *Phys. Rev.* D **88** 075010
[143] Garcia-Pepin M and Quiros M 2016 Strong electroweak phase transition from Supersymmetric Custodial Triplets *J. High Energy Phys.* **2016** 177
[144] Vega R, Vega-Morales R and Xie K 2018 The supersymmetric Georgi–Machacek model *J. High Energy Phys.* **2018** 168
[145] Creminelli P, Nicolis A and Rattazzi R 2002 Holography and the electroweak phase transition *J. High Energy Phys.* **2002** 051
[146] Randall L and Servant G 2007 Gravitational waves from warped spacetime *J. High Energy Phys.* **2007** 054
[147] Hassanain B, March-Russell J and Schvellinger M 2007 Warped deformed throats have faster (electroweak) phase transitions *J. High Energy Phys.* **2007** 089
[148] Nardini G, Quiros M and Wulzer A 2007 A confining strong first-order electroweak phase transition *J. High Energy Phys.* **2007** 077
[149] Konstandin T, Nardini G and Quiros M 2010 Gravitational backreaction effects on the holographic phase transition *Phys. Rev.* D **82** 083513

[150] Konstandin T and Servant G 2011 Cosmological consequences of nearly conformal dynamics at the TeV scale *J. Cosmol. Astropart. Phys.* **2011** JCAP12(2011)009

[151] Servant G 2014 Baryogenesis from Strong CP Violation and the QCD Axion *Phys. Rev. Lett.* **113** 171803

[152] Chen Y, Huang M and Yan Q-S 2018 Gravitation waves from QCD and electroweak phase transitions *J. High Energy Phys.* **2018** 178

[153] Dillon B M, El-Menoufi B K, Huber S J and Manuel J P 2018 Rapid holographic phase transition with brane-localized curvature *Phys. Rev.* D **98** 086005

[154] Bunk D, Hubisz J and Jain B 2018 A perturbative RS I cosmological phase transition *Eur. Phys. J.* C **78** 78

[155] Marzola L, Racioppi A and Vaskonen V 2017 Phase transition and gravitational wave phenomenology of scalar conformal extensions of the Standard Model *Eur. Phys. J.* C **77** 484

[156] Iso S, Serpico P D and Shimada K 2017 QCD-electroweak first-order phase transition in a supercooled universe *Phys. Rev. Lett.* **119** 141301

[157] von Harling B and Servant G 2018 QCD-induced electroweak phase transition *J. High Energy Phys.* **2018** 159

[158] Megías E, Nardini G and Quirós M 2018 Cosmological phase transitions in warped space: gravitational waves and collider signatures *J. High Energy Phys.* **2018** 095

[159] Fujikura K, Nakai Y and Yamada M 2020 A more attractive scheme for radion stabilization and supercooled phase transition *J. High Energy Phys.* **2020** 111

[160] Agashe K, Du P, Ekhterachian M, Kumar S and Sundrum R 2021 Phase transitions from the fifth dimension *J. High Energy Phys.* **2021** 051

[161] Azatov A and Vanvlasselaer M 2020 Phase transitions in perturbative walking dynamics *J. High Energy Phys.* **2020** 085

[162] Bigazzi F, Caddeo A, Cotrone A L and Paredes A 2020 Fate of false vacua in holographic first-order phase transitions *J. High Energy Phys.* **2020** 200

[163] Megías E, Nardini G and Quirós M 2020 Gravitational imprints from heavy kaluza-klein resonances *Phys. Rev.* D **102** 055004

[164] Espinosa J R, Konstandin T, No J M and Quirós M 2008 Some cosmological implications of hidden sectors *Phys. Rev.* D **78** 123528

[165] Iso S, Okada N and Orikasa Y 2009 Classically conformal *B* L extended Standard Model *Phys. Lett.* B **676** 81–7

[166] Iso S, Okada N and Orikasa Y 2009 The minimal *B–L* model naturally realized at TeV scale *Phys. Rev.* D **80** 115007

[167] Okada H and Orikasa Y 2016 Classically conformal radiative neutrino model with gauged *B–L* symmetry *Phys. Lett.* B **760** 558–64

[168] Dorsch G C, Huber S J and No J M 2014 Cosmological Signatures of a UV-Conformal Standard Model *Phys. Rev. Lett.* **113** 121801

[169] Farzinnia A and Ren J 2014 Higgs partner searches and dark matter phenomenology in a classically scale invariant higgs boson sector *Phys. Rev.* D **90** 015019

[170] Farzinnia A and Ren J 2014 Strongly First-Order Electroweak Phase Transition and Classical Scale Invariance *Phys. Rev.* D **90** 075012

[171] Jaeckel J, Khoze V V and Spannowsky M 2016 Hearing the signal of dark sectors with gravitational wave detectors *Phys. Rev.* D **94** 103519

[172] Hashino K, Kakizaki M, Kanemura S and Matsui T 2016 Synergy between measurements of gravitational waves and the triple-Higgs coupling in probing the first-order electroweak phase transition *Phys. Rev.* D **94** 015005

[173] Jinno R and Takimoto M 2017 Probing a classically conformal *B–L* model with gravitational waves *Phys. Rev.* D **95** 015020

[174] Kubo J and Yamada M 2016 Scale genesis and gravitational wave in a classically scale invariant extension of the standard model *J. Cosmol. Astropart. Phys.* **2016** JCAP12 (2016)001

[175] Chiang C-W and Senaha E 2017 On gauge dependence of gravitational waves from a first-order phase transition in classical scale-invariant $U(1)'$ models *Phys. Lett.* B **774** 489–93

[176] Miura K, Ohki H, Otani S and Yamawaki K 2019 Gravitational waves from walking technicolor *J. High Energy Phys.* **2019** 194

[177] Brdar V, Helmboldt A J and Kubo J 2019 Gravitational waves from first-order phase transitions: LIGO as a window to unexplored seesaw scales *J. Cosmol. Astropart. Phys.* **2019** JCAP02(2019)021

[178] Marzo C, Marzola L and Vaskonen V 2019 Phase transition and vacuum stability in the classically conformal *B–L* model *Eur. Phys. J.* C **79** 601

[179] Prokopec T, Rezacek J and Swiezewska B 2019 Gravitational waves from conformal symmetry breaking *J. Cosmol. Astropart. Phys.* **2019** JCAP02(2019)009

[180] Aoki M and Kubo J 2020 Gravitational waves from chiral phase transition in a conformally extended standard model *J. Cosmol. Astropart. Phys.* **2020** JCAP04(2020)001

[181] Bian L, Cheng W, Guo H-K and Zhang Y 2021 Cosmological implications of a B-L charged hidden scalar: leptogenesis and gravitational waves *Chin. Phys.* C **45** 113104

[182] Mohamadnejad A 2020 Gravitational waves from scale-invariant vector dark matter model: Probing below the neutrino-floor *Eur. Phys. J.* C **80** 197

[183] Kang Z and Zhu J 2020 Scale-genesis by dark matter and its gravitational wave signal *Phys. Rev.* D **102** 053011

[184] Chishtie F A, Huang Z-R, Reimer M, Steele T G and Wang Z-W 2020 Transformation of scalar couplings between Coleman–Weinberg and MS schemes *Phys. Rev.* D **102** 076021

[185] Schwaller P, Tait T M P and Vega-Morales R 2013 Dark matter and vectorlike leptons from gauged lepton number *Phys. Rev.* D **88** 035001

[186] Addazi A 2017 Limiting first order phase transitions in dark gauge sectors from gravitational waves experiments *Mod. Phys. Lett.* A **32** 1750049

[187] Hambye T and Strumia A 2013 Dynamical generation of the weak and dark matter scale *Phys. Rev.* D **88** 055022

[188] Baker M J and Kopp J 2017 Dark matter decay between phase transitions at the weak scale *Phys. Rev. Lett.* **119** 061801

[189] Aoki M, Goto H and Kubo J 2017 Gravitational waves from hidden QCD phase transition *Phys. Rev.* D **96** 075045

[190] Addazi A and Marciano A 2018 Gravitational waves from dark first order phase transitions and dark photons *Chin. Phys.* C **42** 023107

[191] Tsumura K, Yamada M and Yamaguchi Y 2017 Gravitational wave from dark sector with dark pion *J. Cosmol. Astropart. Phys.* **2017** JCAP07(2017)044

[192] Baldes I 2017 Gravitational waves from the asymmetric-dark-matter generating phase transition *J. Cosmol. Astropart. Phys.* **2017** JCAP05(2017)028

[193] Baker M J, Breitbach M, Kopp J and Mittnacht L 2018 Dynamic freeze-in: impact of thermal masses and cosmological phase transitions on dark matter production *J. High Energy Phys.* **2018** 114

[194] Bian L and Liu X 2019 Two-step strongly first-order electroweak phase transition modified FIMP dark matter, gravitational wave signals, and the neutrino mass *Phys. Rev.* D **99** 055003

[195] Breitbach M, Kopp J, Madge E, Opferkuch T and Schwaller P 2019 Dark, cold, and noisy: constraining secluded hidden sectors with gravitational waves *J. Cosmol. Astropart. Phys.* **2019** JCAP07(2019)007

[196] Baldes I and Garcia-Cely C 2019 Strong gravitational radiation from a simple dark matter model *J. High Energy Phys.* **2019** 190
[197] Croon D, Sanz V and White G 2018 Model discrimination in gravitational wave spectra from dark phase transitions *J. High Energy Phys.* **2018** 203
[198] Madge E and Schwaller P 2019 Leptophilic dark matter from gauged lepton number: Phenomenology and gravitational wave signatures *J. High Energy Phys.* **2019** 048
[199] Bian L and Tang Y-L 2018 Thermally modified sterile neutrino portal dark matter and gravitational waves from phase transition: The Freeze-in case *J. High Energy Phys.* **2018** 006
[200] Croon D and White G 2018 Exotic gravitational wave signatures from simultaneous phase transitions *J. High Energy Phys.* **05** 210
[201] Hall E, Konstandin T, McGehee R and Murayama H 2019 Asymmetric matters from a dark first-order phase transition *Phys. Rev.* D **107** 055011
[202] Fairbairn M, Hardy E and Wickens A 2019 Hearing without seeing: gravitational waves from hot and cold hidden sectors *J. High Energy Phys.* **2019** 044
[203] Katz A and Riotto A 2016 Baryogenesis and gravitational waves from runaway bubble collisions *J. Cosmol. Astropart. Phys.* **2016** JCAP11(2016)011
[204] Long A J, Tesi A and Wang L-T 2017 Baryogenesis at a lepton-number-breaking phase transition *J. High Energy Phys.* **2017** 095
[205] Archer-Smith P, Linthorne D and Stolarski D 2020 Gravitational Wave Signals from Multiple Hidden Sectors *Phys. Rev.* D **101** 095016
[206] Greljo A, Opferkuch T and Stefanek B A 2020 Gravitational imprints of flavor hierarchies *Phys. Rev. Lett.* **124** 171802
[207] Helmboldt A J, Kubo J and van der Woude S 2019 Observational prospects for gravitational waves from hidden or dark chiral phase transitions *Phys. Rev.* D **100** 055025
[208] Schwaller P 2015 Gravitational waves from a dark phase transition *Phys. Rev. Lett.* **115** 181101
[209] Corian C, Frampton P H and Tatullo A 2020 Conformal unification in a quiver theory and gravitational waves *Phys. Lett.* B **811** 135909
[210] Huang W-C, Sannino F and Wang Z-W 2020 Gravitational waves from pati-salam dynamics *Phys. Rev.* D **102** 095025
[211] Craig N, Levi N, Mariotti A and Redigolo D 2020 Ripples in spacetime from broken supersymmetry *J. High Energy Phys.* **2021** 184
[212] Chao W, Cui W-F, Guo H-K and Shu J 2020 Gravitational wave imprint of new symmetry breaking *Chin. Phys.* C **44** 123102
[213] Huang F P and Zhang X 2019 Probing the gauge symmetry breaking of the early universe in 3-3-1 models and beyond by gravitational waves *Phys. Lett.* B **788** 288–94
[214] Addazi A, Cai Y-F and Marciano A 2018 Testing dark matter models with radio telescopes in light of gravitational wave astronomy *Phys. Lett.* B **782** 732–6
[215] Addazi A and Marciano A 2018 Limiting majoron self-interactions from gravitational wave experiments *Chin. Phys.* C **42** 023105
[216] Ayyar V, DeGrand T, Hackett D C, Jay W I, Neil E T, Shamir Y and Svetitsky B 2018 Finite-temperature phase structure of SU(4) gauge theory with multiple fermion representations *Phys. Rev.* D **97** 114502
[217] Okada N and Seto O 2018 Probing the seesaw scale with gravitational waves *Phys. Rev.* D **98** 063532
[218] Hashino K, Kakizaki M, Kanemura S, Ko P and Matsui T 2018 Gravitational waves from first order electroweak phase transition in models with the U(1)X gauge symmetry *J. High Energy Phys.* **2018** 088
[219] Hasegawa T, Okada N and Seto O 2019 Gravitational waves from the minimal gauged $U(1)_{BL}$ model *Phys. Rev.* D **99** 095039
[220] Hall E, Konstandin T, McGehee R, Murayama H and Servant G 2020 Baryogenesis from a dark first-order phase transition *J. High Energy Phys.* **2020** 042
[221] Azatov A, Barducci D and Sgarlata F 2020 Gravitational traces of broken gauge symmetries *J. Cosmol. Astropart. Phys.* **2020** JCAP07(2020)027
[222] Haba N and Yamada T 2020 Gravitational waves from phase transition in minimal SUSY $U(1)_{BL}$ model *Phys. Rev.* D **101** 075027
[223] Ghosh T, Guo H-K, Han T and Liu H 2021 Electroweak phase transition with an SU(2) dark sector *J. High Energy Phys.* **2021** 045
[224] Okada N, Seto O and Uchida H 2021 Gravitational waves from breaking of an extra U(1) in $SO(10)$ grand unification *PTEP* **2021** 033B01
[225] Halverson J, Long C, Maiti A, Nelson B and Salinas G 2021 Gravitational waves from dark Yang–Mills sectors *J. High Energy Phys.* **2021** 154
[226] Bhupal Dev P S and Mazumdar A 2016 Probing the scale of new physics by advanced LIGO/VIRGO *Phys. Rev.* D **93** 104001
[227] Rose L D, Panico G, Redi M and Tesi A 2020 Gravitational waves from supercool axions *J. High Energy Phys.* **2020** 025
[228] Von Harling B, Pomarol A, Pujols O and Rompineve F 2020 Peccei-quinn phase transition at LIGO *J. High Energy Phys.* **2020** 195
[229] Croon D, Houtz R and Sanz V 2019 Dynamical axions and gravitational waves *J. High Energy Phys.* **2019** 146
[230] Dev P S B, Ferrer F, Zhang Y and Zhang Y 2019 Gravitational waves from first-order phase transition in a simple axion-like particle model *J. Cosmol. Astropart. Phys.* **2019** JCAP11(2019)006
[231] Machado C S, Ratzinger W, Schwaller P and Stefanek B A 2020 Gravitational wave probes of axionlike particles *Phys. Rev.* D **102** 075033
[232] Chiang C-W and Lu B-Q 2021 Testing clockwork axion with gravitational waves *J. Cosmol. Astropart. Phys.* **2021** JCAP05(2021)049
[233] Ghoshal A and Salvio A 2020 Gravitational waves from fundamental axion dynamics *J. High Energy Phys.* **2020** 049
[234] Boeckel T and Schaffner-Bielich J 2010 A little inflation in the early universe at the QCD phase transition *Phys. Rev. Lett* **105** 041301
[235] Schettler S, Boeckel T and Schaffner-Bielich J 2011 Imprints of the QCD phase transition on the spectrum of gravitational waves *Phys. Rev.* D **83** 064030
[236] Boeckel T and Schaffner-Bielich J 2012 A little inflation at the cosmological QCD phase transition *Phys. Rev.* D **85** 103506
[237] Capozziello S, Khodadi M and Lambiase G 2019 The quark chemical potential of QCD phase transition and the stochastic background of gravitational waves *Phys. Lett.* B **789** 626–33
[238] Khodadi M, Nozari K, Abedi H and Capozziello S 2018 Planck scale effects on the stochastic gravitational wave background generated from cosmological hadronization transition: A qualitative study *Phys. Lett.* B **783** 326–33
[239] Bai Y and Long A J 2018 Six flavor quark matter *J. High Energy Phys.* **2018** 072
[240] Bigazzi F, Caddeo A, Cotrone A L and Paredes A 2021 Dark holograms and gravitational waves *J. High Energy Phys.* **2021** 094
[241] Huang W-C, Reichert M, Sannino F and Wang Z-W 2021 Testing the dark SU(N) Yang–Mills theory confined

landscape: From the lattice to gravitational waves *Phys. Rev.* D **104** 035005
[242] Reichert M, Sannino F, Wang Z-W and Zhang C 2022 Dark confinement and chiral phase transitions: gravitational waves vs matter representations *J. High Energy Phys.* **2022** 003
[243] Baldes I and Servant G 2018 High scale electroweak phase transition: baryogenesis & symmetry non-restoration *J. High Energy Phys.* **2018** 053
[244] Glioti A, Rattazzi R and Vecchi L 2019 Electroweak baryogenesis above the electroweak scale *J. High Energy Phys.* **2019** 027
[245] Meade P and Ramani H 2019 Unrestored electroweak symmetry *Phys. Rev. Lett.* **122** 041802
[246] Matsedonskyi O and Servant G 2020 High-temperature electroweak symmetry non-restoration from new fermions and implications for baryogenesis *J. High Energy Phys.* **2020** 012
[247] Cao Q-H, Hashino K, Li X-X, Ren Z and Yu J-H 2022 Electroweak phase transition triggered by fermion sector *J. High Energy Phys.* **2022** 001
[248] Postma M and White G 2021 Cosmological phase transitions: is effective field theory just a toy? *J. High Energy Phys.* **2021** 280
[249] Camargo-Molina José Eliel, Enberg R and Löfgren J 2021 A new perspective on the electroweak phase transition in the Standard Model Effective Field Theory *J. High Energy Phys.* **2021** 127
[250] Gould O, Kozaczuk J, Niemi L, Ramsey-Musolf M J, Tenkanen T V I and Weir D J 2019 Nonperturbative analysis of the gravitational waves from a first-order electroweak phase transition *Phys. Rev.* D **100** 115024
[251] Kainulainen K, Keus V, Niemi L, Rummukainen K, Tenkanen T V I and Vaskonen V 2019 On the validity of perturbative studies of the electroweak phase transition in the Two Higgs Doublet model *J. High Energy Phys.* **2019** 075
[252] Niemi L, Schicho P and Tenkanen T V I 2021 Singlet-assisted electroweak phase transition at two loops *Phys. Rev.* D **103** 115035
[253] Croon D, Gould O, Schicho P, Tenkanen T V I and White G 2021 Theoretical uncertainties for cosmological first-order phase transitions *J. High Energy Phys.* **2021** 055
[254] Gould O and Tenkanen T V I 2021 On the perturbative expansion at high temperature and implications for cosmological phase transitions *J. High Energy Phys.* **2021** 069
[255] Gould O and Hirvonen J 2021 Effective field theory approach to thermal bubble nucleation *Phys. Rev.* D **104** 096015
[256] Löfgren J, Ramsey-Musolf M J, Schicho P and Tenkanen T V I 2021 Nucleation at finite temperature: a gauge-invariant, perturbative framework *Phys. Rev. Lett.* **130** 251801
[257] Hirvonen J, Löfgren J, Ramsey-Musolf M J, Schicho P and Tenkanen T V I 2021 Computing the gauge-invariant bubble nucleation rate in finite temperature effective field theory *J. High Energy Phys.* **2022** 135
[258] Coleman S R and Weinberg E J 1973 Radiative corrections as the origin of spontaneous symmetry breaking *Phys. Rev.* D **7** 1888–910
[259] Gildener E and Weinberg S 1976 Symmetry breaking and scalar bosons *Phys. Rev.* D **13** 3333
[260] Endo K and Sumino Y 2015 A scale-invariant higgs sector and structure of the vacuum *J. High Energy Phys.* **2015** 030
[261] Hally K, Logan H E and Pilkington T 2012 Constraints on large scalar multiplets from perturbative unitarity *Phys. Rev.* D **85** 095017
[262] Earl K, Hartling K, Logan H E and Pilkington T 2013 Constraining models with a large scalar multiplet *Phys. Rev.* D **88** 015002
[263] Aad G *et al* 2020 Combined measurements of Higgs boson production and decay using up to 80 fb^{-1} of proton-proton collision data at $\sqrt{s} = 13$ TeV collected with the ATLAS experiment *Phys. Rev.* D **101** 012002
[264] Henning B, Lu X and Murayama H 2016 How to use the Standard Model effective field theory *J. High Energy Phys.* **01** 023
[265] Dolan L and Jackiw R 1974 Symmetry behavior at finite temperature *Phys. Rev.* D **9** 3320–41
[266] Carrington M E 1992 The Effective potential at finite temperature in the Standard Model *Phys. Rev.* D **45** 2933–44
[267] Hashino K, Kanemura S and Orikasa Y 2016 Discriminative phenomenological features of scale invariant models for electroweak symmetry breaking *Phys. Lett.* B **752** 217–20
[268] Coleman S R 1977 The fate of the false vacuum. 1. semiclassical theory *Phys. Rev.* D **15** 2929–36
[269] Callan Jr. C G and Coleman S R 1977 The fate of the false vacuum. 2. first quantum corrections *Phys. Rev.* D **16** 1762–8
[270] Linde A D 1981 Fate of the false vacuum at finite temperature: theory and applications *Phys. Lett.* **100B** 37–40
[271] Linde A D 1981 Decay of the false vacuum at finite temperature *Phys. Lett.* **100B** 37–40
[272] Guth A H and Weinberg E J 1983 Could the universe have recovered from a slow first order phase transition? *Nucl. Phys.* B **212** 321–64
[273] Turner M S, Weinberg E J and Widrow L M 1992 Bubble nucleation in first order inflation and other cosmological phase transitions *Phys. Rev.* D **46** 2384–403
[274] Ellis J, Lewicki M and No José Miguel 2019 On the maximal strength of a first-order electroweak phase transition and its gravitational wave signal *J. Cosmol. Astropart. Phys.* **2019** JCAP04(2019)003
[275] Ellis J, Lewicki M and No J M 2020 Gravitational waves from first-order cosmological phase transitions: lifetime of the sound wave source *J. Cosmol. Astropart. Phys.* **2020** JCAP07(2020)050
[276] Wang X, Huang F P and Zhang X 2020 Phase transition dynamics and gravitational wave spectra of strong first-order phase transition in supercooled universe *J. Cosmol. Astropart. Phys.* **2020** JCAP05(2020)045
[277] Kosowsky A, Turner M S and Watkins R 1992 Gravitational radiation from colliding vacuum bubbles *Phys. Rev.* D **45** 4514–35
[278] Kosowsky A, Turner M S and Watkins R 1992 Gravitational waves from first order cosmological phase transitions *Phys. Rev. Lett.* **69** 2026–9
[279] Kosowsky A and Turner M S 1993 Gravitational radiation from colliding vacuum bubbles: envelope approximation to many bubble collisions *Phys. Rev.* D **47** 4372
[280] Kamionkowski M, Kosowsky A and Turner M S 1994 Gravitational radiation from first order phase transitions *Phys. Rev.* D **49** 2837
[281] Huber S J and Konstandin T 2008 Gravitational wave production by collisions: more bubbles *J. Cosmol. Astropart. Phys.* **2008** JCAP09(2008)022
[282] Hindmarsh M, Huber S J, Rummukainen K and Weir D J 2014 Gravitational waves from the sound of a first order phase transition *Phys. Rev. Lett.* **112** 041301
[283] Hindmarsh M, Huber S J, Rummukainen K and Weir D J 2015 Numerical simulations of acoustically generated gravitational waves at a first order phase transition *Phys. Rev.* D **92** 123009
[284] Hindmarsh M, Huber S J, Rummukainen K and Weir D J 2017 Shape of the acoustic gravitational wave power spectrum from a first order phase transition *Phys. Rev.* D **96** 103520
[285] Cutting D, Hindmarsh M and Weir D J 2020 Vorticity, kinetic energy, and suppressed gravitational wave production in

strong first order phase transitions *Phys. Rev. Lett.* **125** 021302
[286] Guo H-K, Sinha K, Vagie D and White G 2021 Phase transitions in an expanding universe: stochastic gravitational waves in standard and non-standard histories *J. Cosmol. Astropart. Phys.* **2021** JCAP01(2021)001
[287] Espinosa J R, Konstandin T, No J M and Servant G 2010 Energy budget of cosmological first-order phase transitions *J. Cosmol. Astropart. Phys.* **2010** JCAP06(2010)028
[288] Corbett T, Joglekar A, Li H-L and Yu J-H 2018 Exploring extended scalar sectors with di-Higgs signals: a higgs EFT perspective *J. High Energy Phys.* **2018** 061
[289] Li H-L, Ren Z, Shu J, Xiao M-L, Yu J-H and Zheng Y-H 2021 Complete set of dimension-eight operators in the standard model effective field theory *Phys. Rev.* D **104** 015026
[290] Li H-L, Ren Z, Xiao M-L, Yu J-H and Zheng Y-H 2021 Complete set of dimension-nine operators in the standard model effective field theory *Phys. Rev.* D **104** 015025
[291] Hill C T 2014 Is the higgs boson associated with Coleman–Weinberg dynamical symmetry breaking? *Phys. Rev.* D **89** 073003
[292] Helmboldt A J, Humbert P, Lindner M and Smirnov J 2017 Minimal conformal extensions of the Higgs sector *J. High Energy Phys.* JHEP07(2017)113
[293] Agrawal P, Saha D, Xu L-X, Yu J-H and Yuan C P 2020 Determining the shape of the Higgs potential at future colliders *Phys. Rev.* D **101** 075023